Cement and Concrete Composites 163 (2025) 106166

Contents lists available at ScienceDirect

Cement and Concrete Composites

journal homepage: www.elsevier.com/locate/cemconcomp

General correlation between R^3 test results and compressive strengths for five families of supplementary cementitious materials

Imane Koufany [a], Angeles G. De la Torre [a], Cinthya Redondo-Soto [a], Isabel Santacruz [a], Ana Cuesta [a], Daniela Gastaldi [b], Fulvio Canonico [b], Oliver Mazanec [c], Miguel A.G. Aranda [a,*]

[a] Departamento de Química Inorgánica, Cristalografía y Mineralogía, Universidad de Málaga, Málaga, 29071, Spain
[b] Buzzi Innovation Lab and Technology, Via Restano 3, 15100, Vercelli, VC, Italy
[c] Master Builders Solutions Deutschland GmbH, Albert-Frank Str. 32, 83308, Trostberg, Germany

A R T I C L E I N F O

Keywords:
Pozzolanic reactivity
Pozzolanic reaction rate
Strength activity index
Blended cements
Smectitic calcined clays
Natural pozzolans
Kaolinitic calcined clay
Fly ash

A B S T R A C T

The incorporation of locally available supplementary cementitious materials (SCMs) in cement blends is essential for reducing the environmental impact of construction. However, assessing the pozzolanic kinetics, and thus the pozzolanic contribution at a given age, is challenging due to temperature differences between the two main evaluation methods: ASTM C1897 (40 °C, continuous heat release) and ASTM C311 (20 °C, Strength Activity Index at 28 days). This study examines 22 SCMs, analysing their composition, mineralogy, texture, and pozzolanic behaviour. ASTM C1897 was applied as prescribed, while ASTM C311 was modified by maintaining a constant water-to-binder ratio and introducing an additional 68 % PC–20 % SCM–10 % limestone–2 % gypsum series to better isolate pozzolan effects. The results confirmed established pozzolanic trends, with kaolinite-rich calcined clays $\gtrsim$ silica fume $>$ smectite-rich calcined clays $>$ natural pozzolans $\gtrsim$ class-F fly ashes. The modified series yielded clearer correlations, particularly between $SAI^{2°C}_{28d}$ and $Heat^{4°C}_{3d}$, forming two well-defined clusters that reflect general behaviour. These findings suggest that the modified series could serve as a more reliable framework for future SAI evaluations. Moreover, for the 80 % PC–20 % SCM, the best correlation is found for the R^3-heat release at 12 h (at 40 °C) and the SAI values at 28 days (at 20 °C). Additional insights into the pozzolanic kinetics and performance of the materials are also presented, contributing to a deeper understanding of their potential in sustainable construction practices.

1. Introduction

Cement manufacturing is a contributor to global CO_2 emissions, accounting for approximately 8 % of total greenhouse gas emissions. This poses a critical challenge for the construction industry, which must reduce its carbon footprint while maintaining high material performance standards [1]. The production of Portland cement (PC), the primary component in concrete, is particularly energy-intensive and responsible for substantial CO_2 emissions [2]. In response, the industry has adopted a roadmap to achieve net-zero emissions by 2050. This plan includes interim goals, such as a 25 % reduction in CO_2 emissions by 2030, and outlines key pathways and milestones for full decarbonization [3–6]. Consequently, there is a growing emphasis on identifying low-carbon materials that satisfy both mechanical performance and durability requirements.

Supplementary Cementitious Materials (SCMs) [7,8] play a crucial role in mitigating the environmental impact of cement production. Currently, SCMs are among the most effective strategies for reducing CO_2 emissions. Clinker substitution [9], combined with optimized concrete mixture proportioning, has been particularly effective in lowering the carbon footprint of concrete production. While high-quality SCMs, such as granulated blast furnace slags, have proven highly efficient [7,10], their limited availability necessitates the increased use of other widely available SCMs [8] including calcined clays (CCs) [11–13] and/or natural pozzolans (NPs) [14,15]. Coal combustion fly ashes (FAs) [16] and silica fume (SF) [17,18] are also widely utilized as SCMs and serve as key references for pozzolanic materials with slow and fast reaction kinetics, respectively. Although kaolinitic calcined clays (KCCs) are receiving significant attention due to their fast pozzolanic kinetics [11,19–27], other clay-based SCMs have not been studied as extensively. This work focuses on the pozzolanic features of five SCM families: kaolinitic CC (KCCs), smectitic CC (SCCs), SFs, NPs, and FAs. A brief

* Corresponding author.
E-mail address: g_aranda@uma.es (M.A.G. Aranda).

https://doi.org/10.1016/j.cemconcomp.2025.106166
Received 13 December 2024; Received in revised form 28 March 2025; Accepted 3 June 2025
Available online 4 June 2025

discussion of these materials' pozzolanic properties follows in the subsequent paragraphs.

Among clay minerals, kaolinite and smectite are the primary focus due to their distinct compositions, structures, and pozzolanic properties when (so far, thermally) activated as meta-clays [12,25]. Thermal activation involves dehydroxylating the octahedral sheet, forming amorphous meta-clays while avoiding recrystallization at elevated temperatures [12].

Briefly, kaolinite features a 1:1 layered structure comprising one tetrahedral (silicate) layer and one octahedral (aluminate) layer, with an ideal chemical stoichiometry of $Al_4Si_4O_{10}(OH)_8$. Upon calcination at 600–900 °C (optimal range: ~700–850 °C), kaolinite phase transforms into metakaolin (MK) with an ideal stoichiometry of $Al_2Si_2O_7$. This transformation significantly enhances its pozzolanic activity, making MK highly effective in cementitious applications [28,29]. Notably, MK exhibits the fastest pozzolanic reaction kinetics among SCMs. In contrast, smectite minerals have a 2:1 structure, consisting of two tetrahedral (silicate) sheets and one octahedral layer. Smectites are further classified into dioctahedral (trivalent cations) and trioctahedral (divalent cations) types based on the composition of the octahedral layer [30,31]. Montmorillonite, a dioctahedral smectite with primarily aluminate octahedral layers, has an ideal stoichiometry of $Al_2Si_4O_{10}(OH)_2nH_2O$, with inherent lower aluminium content when compared to kaolinite clays. Moreover, elemental substitutions lead to a range of stoichiometries, such as Na-montmorillonite, $\approx Na_{0.3}(Al_{1.7}Mg_{0.2}Fe_{0.1})Si_4O_{10}(OH)_2nH_2O$. Interlayer cations like calcium result in Ca-montmorillonite, while trioctahedral smectites, where magnesium dominates the octahedral layer, are classified as saponites with an approximate formula of $\approx (Ca,Na)_{0.3}(Mg,Fe)_3Si_4O_{10}(OH)_2nH_2O$. Montmorillonites, part of the smectite family, are commonly found in bentonite rocks. When calcined, smectites yield meta-clays with variable Al/Si molar ratios, typically ranging from 0.45:1 in Al-rich smectites to 0.20:1 in Al-poor smectites. The lower Al/Si ratio of calcined smectite has a direct impact in the hydration behaviour of blended cements [32]. The calcination temperature for smectitic clays ranges 750–900 °C, with an optimal range narrower than that of kaolinitic clays [16]. Recent studies [33] has reported that calcined Ca- and Na-montmorillonites can be considered as medium to high reactivity SCMs according to their heat at 7 d, determined by the ASTM C1897 standard [34]. Moreover, there is a growing interest on the role of smectites as SCM [35].

Silica fume (SF) is widely regarded as one of the most effective pozzolanic materials, significantly enhancing the compressive strength, durability, and chemical resistance of concretes [36,37]. This by-product of silicon and ferrosilicon production is primarily composed of SiO_2. SF features extremely fine particle sizes, typically smaller than 0.5 μm, and a very high specific surface area [8]. For safer handling, SF particles are often deliberately agglomerated. In concrete applications, SF is used in relatively small quantities, where it fills voids, reduces porosity, and increases density. These properties make SF particularly valuable in high-performance concrete applications [36,37].

Natural pozzolans (NPs) are siliceous or alumino-siliceous materials that, when processed (e.g., milled), chemically react with $Ca(OH)_2$ under ambient conditions to form compounds with cementitious properties [14,15,38–42]. NPs are formed during volcanic eruptions, where magma reaches the surface and expanding gases cause explosive eruptions, producing fine ash and rapidly cooling lava. Volcanic materials, such as pumice (lava rock) and pumicite (volcanic dust), primarily consist of aluminosilicate glass with minor amounts of minerals, including quartz, feldspar, and mica [43]. Over time, volcanic glass may transform into volcanic tuff, which is rich in zeolite minerals. These natural pozzolans exhibit pozzolanic properties with variable, often slow, reaction kinetics and have been used in construction since Roman times [14,40,44].

Coal fly ashes (FAs) are by-products of coal combustion in power plants, consisting of fine particles collected from flue gases. FAs are widely utilized as SCMs in concrete to enhance durability and reduce the Portland cement (PC) content, thereby lowering the carbon footprint of construction materials [45–47]. FAs are generally classified into two categories: Class-F and Class-C, each characterized by distinct compositions, properties, and applications. Class-F FAs are calcium-poor, exhibiting primarily pozzolanic properties with minimal hydraulic behaviour.

Alongside with well-established and emerging SCMs [8], effective testing methods are essential for assessing their pozzolanic performances. Such performances must to be evaluated at specific time points, making pozzolanic kinetics a critical factor. Several traditional methods exist for determining pozzolanic performances, such as the Frattini test, Chapelle test, and lime-SCM compressive strength test. However, a review of these methods is beyond the scope of this discussion [48–51]. Currently, ASTM evaluates SCM reactivity using the Strength Activity Index (SAI) as defined in the ASTM C311 standard [52], performed at room temperature. This test is used to determine compliance with the ASTM C618 standard [53] for fly ashes and natural pozzolans. According to ASTM C618, SCM mixtures with 20 % replacement must achieve at least 75 % of the control's compressive strength at either 7 or 28 days. Similarly, the European standard EN 450-1 [54] measures the activity index of mortars with 25 % SCM replacement, requiring at least 75 % of the control's compressive strength at 28 days and 85 % at 90 days. While ASTM C618 remains widely used, it has notable limitations in differentiating between inert and pozzolanic materials and in accurately ranking pozzolanic performance [49,55]. This is likely due to the low replacement level (20 %), where filler effects can dominate over pozzolanic contributions. To address these limitations, researchers have developed the R^3 test (rapid, relevant, and reliable), which isolates pozzolanic reactions and provides a faster evaluation of a material's reactivity. The R^3 test has been standardized as ASTM C1897-20 [34,50,56–58]. The R^3 test measures heat release and bound water (BW) in lime-SCM optimized pastes at 40 °C, offering a reliable method to assess pozzolanicity, including pozzolanic kinetics and ultimate performance. These relatively rapid tests are particularly effective in distinguishing pozzolanic materials from inert ones and in determining whether a material warrants further long-term testing, particularly in cases of slow pozzolanic kinetics. A recent study [59] evaluated the pozzolanic activity by ASTM C1897-20 of emerging SCMs, including construction and demolition waste as well as rice husk ash. The study established correlations between chemical composition, amorphous content, and reactivity, highlighting a relationship between the amorphous phase content and cumulative heat release. Based on these findings, a new classification system for pozzolanic reactivity has been proposed, defined according to cumulative heat release at 7 days: low (25–100 J/g), moderate (100–180 J/g), high (180–360 J/g), and very high (>360 J/g). However, thid study did not establish a correlation between pozzolanic reactivity and mechanical strength.

This study focused on evaluating the pozzolanic kinetics and final performance of five families of SCMs using the ASTM C1897-20 standard, referred to as the R^3 test. The primary objective was to correlate the outputs of the R^3 test with the compressive strengths of the corresponding blends. Previous attempts have been made to establish such correlations. RILEM TC 267-TRM [57] reported a linear correlation between the relative compressive strength (measured at room temperature and 28 days) and the heat released at 40 °C over 7 days for 52 materials [57]. The compressive strengths were determined at 30 % SCM replacement (10 % for SF) to maximize pozzolanic contributions while minimizing filler effects. Interestingly, two distinct trends were observed: one comprising natural pozzolans (NPs), fly ashes (FAs), and slags, and another including only kaolinitic calcined clays. The cumulative heat release showed R^2 values of 0.87 and 0.84 for the first and second clusters, respectively. Notably, the slope of the first cluster (0.095) was twice that of the second (0.047), indicating that for the same heat release, NPs and FAs achieved higher compressive strengths compared to kaolinitic calcined clays. Yoon et al. [60] also explored these correlations for eleven SCMs, but compressive strengths were

Table 1
Overview and abbreviation of the employed materials.

Material code	Country of origin	Content	Calcination details
KRC1	Spain	≈74 wt% Kln	860 °C/4 h
KRC2	France	≈54 wt% Kln	800 °C/4 h
KRC3	Spain	≈58 wt% Kln	860 °C/4 h
KRC4	Spain	≈48 wt% Kln	860 °C/4 h
KRC5	Spain	≈40 wt% Kln	860 °C/4 h
KRC6	Spain	≈40 wt% Kln	860 °C/4 h
KRC7	Spain	≈20 wt% Kln	860 °C/4 h
Ref1-SRC (SAu-1)	Clay Minerals Society, USA	≈93 wt% Smt-Al	750 °C/2 h
Ref2-SRC (SWy-3)	Clay Minerals Society, USA	≈75 wt% Smt-Al	800 °C/2 h
SRC1	Spain	≈80 wt% Smt-Mg	850 °C/2 h
SRC2	Spain	≈74 wt% Smt-Al	850 °C/2 h
SRC3	Morocco	≈53 wt% Smt-Al	800 °C/2 h
SF1	Spain	–	–
SF2	Spain	–	–
NP1	Greece	–	–
NP2	Italy	–	–
NP3	Spain	–	–
NP4	Germany	–	–
NP5	Spain	–	–
NP6	Italy	–	–
FA1 (Class-F)	Spain	–	–
FA2 (Class-F)	Spain	–	–
Qz (Quartz)	Spain	–	–
LS (Limestone)	Spain	–	–
Gyp (Gypsum)	Spain	–	–
PC (CEM I 52.5 R)	Italy	–	–

evaluated at 20 % SCM replacement, with slight variations in the water-to-binder (w/b) ratio to maintain consistent workability. In this case, the correlation between the SAI at 28 days and the heat released was found to be very poor [60]. It has also been recently identified a strong correlation between the compressive strength of mortars incorporating 30 wt% natural volcanic pozzolan (w/b = 0.40) and the bound water content determined via a modified R^3 protocol [61]. This modification involved adjusting the sulfate and alkali contents to attain a pore solution pH of 13.3. Moreover, a small-scale modified R^3 test has been reported for new SCMs which are initially available only in small quantities [62].

Here, we report a thorough study of 22 SCMs alongside one inert reference material (i.e. quartz with $D_{V,50}$ = 15.5 μm). The SCMs were categorized into five families: KCCs, SCCs, SFs, NPs, and FAs. Following elemental and mineralogical analyses, the raw materials were thermally activated when needed, i.e. kaolinitic and smectitic clays. The SCMs were then milled to achieve similar particle sizes, targeting a $D_{V,50}$ of 12 ± 2 μm. Two experimental campaigns were conducted. In the first, R^3 tests were performed on all SCMs, with extended measurements up to 14 days for selected SCMs to examine longer-term pozzolanic behaviour. Additionally, SAI measurements were carried out using 80/20 blends of Portland cement (PC) and SCMs with a constant water-to-binder (w/b) ratio. For selected blends, SAI values were also measured at 180 days to gain insights into long-term pozzolanic properties. In the second campaign, SAI measurements were conducted for 68/20/10/2 blends, consisting of 68 wt% PC, 20 wt% SCM, 10 wt% limestone (LS), and 2 wt % gypsum (Gyp). This blend composition was designed to minimize filler effects and better reflect current industrial practices, profiting from the wide limestone availability. Finally, the core focus of this study was to establish correlations between the SAI values (measured at 20 °C) and R^3 test results (measured at 40 °C). The findings reveal a strong correlation between $SAI^{2\circ C}_{28d}$ values and the $Heat^{4\circ C}_{3d}$ results for the 68/20/10/2 blends. Kaolinitic calcined clays formed a distinct cluster with a smaller slope, while smectitic calcined clays aligned closely with the FAs, NPs, and SFs cluster. Furthermore, an in-depth analysis of the pozzolanic kinetics across the different SCM families was conducted, providing valuable insights into their reactivity and performances.

2. Materials and methods

2.1. Material provenances

A total of twenty-seven materials were used here, including 22 SCMs with very different pozzolanic kinetics and final performances. The studied SCMs are grouped in: (i) seven kaolinitic raw clays (KRCs); (ii) five smectitic raw clays (SRCs) [two were reference materials from the Clay Minerals Society]; (iii) two SF samples; (iv) six NPs; and (v) two class-F FAs. In addition, five other materials were also employed: inert quartz, limestone (LS), gypsum (Gyp), PCs 52.5R and standard sand. Table 1 provides an overview of the abbreviations for each material, along with the kaolinite and smectite contents of the pristine clays and the thermal activation parameters, where applicable. All materials were dried at 105 °C prior to analysis and usage. The kaolinite and smectite contents were determined using a previously reported methodology [12,63,64], and the clays were thermally activated to produce the SCMs following established protocols [64–66].

Two distinct blends/series were prepared. Blend 80/20 consisted of 80 wt% of PC and 20 wt% of SCM. Blend 68/20/10/2 comprised 68 wt% of PC, 20 wt% of SCM, 10 wt% LS and 2 wt% of Gyp. The blends were homogenized using a Micro-Deval mill (Proeti) equipped with five steel balls, each 32 mm in diameter. It is important to note that this equipment was utilized for mixing rather than milling. To ensure uniformity, each blend underwent 2 × 90 min mixing cycles, with 30 min pause in between. Three batches were prepared for each blend, which were subsequently combined.

Additionally, a commercial polycarboxylate-ether (PCE) superplasticizer, MasterSuna SBS 3890, provided by Master Builders Solutions, was employed and is referred to as PCE.

2.2. Methods

2.2.1. X-ray fluorescence analysis (XRF)

The elemental composition analyses were conducted using an ARL ADVANT'XP + instrument (Thermo Fisher) at the Servicios Centrales de Apoyo a la Investigación (SCAI), University of Malaga. The samples were prepared as fused beads. Loss on ignition (LOI) was determined by heating the samples to 950 °C for 2 h.

2.2.2. Laboratory X-ray powder diffraction (LXRPD)

All raw and calcined materials were analysed by LXRPD. To quantify amorphous and unquantified crystalline phases (ACn) in the samples following the method described in Ref. [67], the specimens were mixed with 20 wt% of α-Al_2O_3 or ZnO (as internal standards). The mixtures were ground in an agate mortar for 15 min to ensure homogenous distribution of the internal standard. Powder diffraction patterns were obtained using two different powder diffractometers at the SCAI, depending on instrument availability. The first, a PANalytical X'Pert PRO MPD, operates in a Bragg-Brentano configuration with monochromatic Cu-Kα_1 radiation (1.5406 Å). The second, a Bruker AXS D8 ADVANCE, uses monochromatic Mo-Kα_1 radiation (0.7093 Å). Rietveld quantitative phase analysis (RQPA) was conducted using GSAS software [68].

2.2.3. Textural characterization techniques

The PSD of the materials was determined using a Malvern Panalytical Mastersizer 3000 equipped with a dry chamber (Aero S). Dry powder particles were dispersed through a high-energy Venturi disperser using compressed air to ensure appropriate sample dispersion. The PSD data were analysed using the MIE non-spherical model, incorporating the specified refractive and absorption indices. In addition, the SSA of the materials was measured through nitrogen adsorption isotherms using the Brunauer-Emmett-Teller (BET) method on an ASAP 2420 analyser (Micromeritics, USA). Sample density was determined via helium pycnometry using an Accupyc II 1320 pycnometer, also from Micromeritics.

2.2.4. Evaluation of pozzolanic reactivity through the R^3 test

The pozzolanic reactivity test was performed in accordance with the ASTM C1897 standard. Each mixture consisted of 10 g of SCM, 30 g of $Ca(OH)_2$, 5 g of $CaCO_3$, and an alkaline sulfate solution containing 4 g/L of KOH and 20 g/L of K_2SO_4. The paste mixtures were prepared with an alkaline solution-to-solid mass ratio of 1.20. The solids and the alkaline solution were sealed in airtight containers and placed in an oven at 40 $\pm$ 2 °C for at least 5 h to ensure thermal stabilization. Mixing was performed using a mechanical stirrer operating at 1600 $\pm$ 50 rpm for 2 min. Following mixing, 15 g of the paste was transferred into a 20 ml glass ampoule, which was then sealed and placed in a TAM Air isothermal calorimeter set to 40 °C. Heat flow measurements, excluding the initial 75 min, were recorded over 7 days, and cumulative heat was calculated per gram of SCM as specified in the standard.

For the BW test, the remaining paste, after the fraction allocated for isothermal calorimetry, was divided into six plastic vials, each containing 5 ml. These vials were sealed and returned to the oven at 40 $\pm$ 2 °C for curing periods of 1 and 7 days. After the specified curing times, the top 5 mm of each paste sample was removed and discarded. Since the mixtures were too soft to crush and sieve, approximately 10 $\pm$ 1 g of each paste was spread into a uniform layer on a Petri dish and placed back in the oven to dry at the same temperature. Once dried, 5 g of each sample was further dehydrated at 350 °C for 2 h and then cooled in a desiccator for 1 h. The BW content for each SCM was calculated following the protocol dictated by ASTM C1897.

2.2.5. Mortars for modified SAI testing

Mortars were cast in 40 $\times$ 40 $\times$ 160 mm^3 moulds to assess the compressive strength of the blended cements and determine the SAI, in accordance with the ASTM C311 standard, with one modification. The water-to-binder (w/b) ratio was maintained at 0.50 to ensure consistent comparisons. Mortars for both blend series were prepared with a water/binder/sand mass ratio of 0.50/1/3. When required, PCE superplasticiser was added to achieve an initial mortar flow of 190 $\pm$ 30 mm. The water, including the required amount of PCE, was magnetically stirred for 1 min before being added to the binder in a single step. During specimen preparation, the moulds were half-filled and tapped 60 times to release trapped air. Once fully filled, the moulds were tapped an additional 60 times on a jolting table (UTCM-0012, 3R Montauban, France) to ensure proper compaction. The samples were left in the moulds for 24 h at 20 °C and 99 % relative humidity before being demoulded and submerged in water at 20 °C. Specimens were cured until compressive strength tests were conducted at 28 days and, in some cases, 180 days.

2.2.6. Slump tests

The same mortar mix described above was used to measure the flow of fresh mortars, following the EN 1015-3 standard. In this test, a metal cone with a base diameter of 100 mm, a top diameter of 70 mm, and a height of 60 mm was placed on a smooth, flat surface. The mortar was poured into the cone, which was then lifted to allow the mortar to spread. The table was jolted 15 times to facilitate the spread, and the diameter of the spread mortar was measured in two perpendicular directions. The average of these two measurements was used to determine the flow of the fresh mortar.

2.2.7. Compressive strengths

Compressive strength testing was conducted in accordance with the EN 196-1 standard, using an Autotest 300/20C MD2-ECO press located at the Universidad de Málaga. Measurements were performed on six half-prisms tested at each time, and the reported compressive strength values represent the average of all measurements.

3. Results

3.1. Elemental and mineralogical compositions

The elemental analyses of all employed material, including the 22 SCMs, are presented in Table 2. Kaolinite and smectite clays underwent thermal activation under previously reported conditions [63–66]. The elemental compositions of the 12 raw clays are given in Table A1 in the Annex. The mineralogical compositions of all SCMs, determined using Rietveld Quantitative Phase Analysis (RQPA) and including amorphous and unquantified crystalline phases (ACn), are shown in Table 3. Additional information on the mineralogical compositions of the raw clays is provided in Table A2. Table A3 summarises the mineralogical phase assemblages of PC, quartz, LS, and Gyp.

3.2. Textural properties

The importance of textural properties is on par with elemental and mineralogical compositions for understanding the reactivity of SCMs. Following the thermal activation of the clays, most SCMs underwent ball milling to achieve comparable particle sizes; however, SFs were not milled. Significant differences in average particle sizes can lead to reactivity variations that obscure general trends. The targeted $D_{v,50}$ particle size was 12 $\pm$ 2 µm. Current practices favour milling SCMs to achieve average particle sizes slightly smaller than that of the employed PC. Fig. 1 shows the PSD of all employed materials, shown as relative volume percentage, while, Fig. 2 illustrates the same distribution as cumulative volume percentages. Table 4 provides the corresponding numerical data, including specific surface areas, densities, and standard PSD values such as $D_{V,10}$, $D_{V,50}$ and $D_{V,90}$. Additionally, Table 4 includes the volume fractions of particles with apparent diameters smaller than 3 µm.

It is noteworthy to underline that silica fume has a primary particle size smaller than 1 µm. However, Figs. 1 and 2 reveal that the measured average particle size of these commercial SFs is significantly larger than 1 µm. This discrepancy arises from the intentional agglomeration of SF by suppliers to minimize handling hazards. Furthermore, the volume fraction of particles smaller than 3 µm ranges from approximately ≈10 to ≈28 vol%; for kaolinitic calcined clays, while for smectitic calcined clays, this fraction is approximately ≈24 vol%.

Table 2
Elemental compositions of all employed materials used in the fabrication of the blends, expressed as oxide weight percentages. Loss on Ignition (LOI) values are also included.

wt%	SiO_2	Al_2O_3	Fe_2O_3	CaO	MgO	K_2O	Na_2O	SO_3	Minors	S + A + F[a]	LOI*
KCC1	54.7	33.5	7.1	0.5	0.1	0.3	–	0.2	2.4	95	1.1
KCC2	68.2	25.9	2.8	0.3	0.1	0.3	0.1	0.04	1.2	97	1.1
KCC3	60.4	32.0	1.3	0.3	0.4	3.6	0.2	0.3	0.7	94	1.0
KCC4	58.9	32.4	1.8	0.04	0.4	5.3	0.3	0.02	0.3	93	0.7
KCC5	76.5	20.5	0.3	0.1	0.1	1.4	–	0.03	0.2	97	1.0
KCC6	81.4	16.4	0.2	0.1	0.1	1.3	–	0.01	0.2	98	0.3
KCC7	66.9	16.4	7.5	1.5	1.1	3.4	0.3	0.3	1.6	91	1.0
Ref1-SCC	62.5	19.2	5.3	0.1	4.4	1.6	1.0	0.2	0.8	87	5.1
Ref2-SCC	67.3	19.7	4.8	1.7	2.3	0.6	1.8	1.0	0.3	92	0.6
SCC1	60.2	9.1	4.8	1.4	18.6	2.5	0.4	0.02	0.8	74	2.2
SCC2	59.6	15.6	6.0	9.9	3.8	1.1	1.2	0.02	0.8	81	2.0
SCC3	60.9	18.1	5.6	3.8	2.5	4.0	2.4	0.2	1.1	85	1.5
SF1	96.8	–	0.2	0.2	0.4	0.9	0.2	0.2	0.2	97	1.0
SF2	90.1	0.7	4.6	0.7	0.5	0.5	1.0	–	0.3	95	1.5
NP1	72.3	11.9	0.8	0.8	0.5	3.9	3.0	0.04	0.2	85	6.5
NP2	48.1	12.9	8.6	11.2	4.2	1.6	1.3	3.1	1.9	70	7.0
NP3	50.9	11.7	10.5	8.8	9.2	1.3	1.5	–	0.9	73	2.6
NP4	54.3	16.9	4.8	5.8	1.6	6.4	3.2	0.3	1.4	76	5.4
NP5	46.0	12.0	11.6	10.2	10.3	1.7	3.0	0.1	1.0	70	1.4
NP6	45.6	14.8	9.3	11.4	4.6	6.5	2.0	0.1	1.9	70	3.9
FA1	44.3	24.8	7.5	3.9	1.7	3.2	0.7	0.6	2.3	77	10.7
FA2	48.5	29.9	3.6	6.8	1.7	0.9	0.3	0.2	3.6	82	4.5
Qz	99.5	–	0.04	–	–	0.1	–	0.1	0.02	–	0.3
LS	–	0.3	0.04	56.0	0.4	–	0.2	0.02	0.03	–	43.1
Gyp	2.1	1.1	0.3	33.1	1.6	0.2	0.1	43.8	0.01	–	17.6
PC	18.7	4.9	3.0	63.9	1.1	0.6	0.21	3.3	0.5	–	3.7

*Dried at 105 °C and heated at 950 °C for 2 h.
[a] S + A + F stands for the sum of SiO_2, Al_2O_3 and Fe_2O_3.

3.3. *Pozzolanic reactivity of the SCMs as measured by R^3 test at 40 °C – isothermal calorimetry*

In this study, the early-age kinetics and long-term performances of the pozzolans were assessed using R^3 measurements. Fig. 3 presents the cumulative heat release, normalised to grams of SCM, over 7 days for the 22 SCMs, along with two inert samples, quartz and the standard sand (UNE-EN 196-1). Additionally, Table 5 provides detailed data on heat release of the studied materials at half, one, three and seven days (at 40 °C). This is reported to follow the kinetics of the pozzolanic reactions in these conditions. Moreover, Fig. A1 shows the heat flow curves up to 48 h for better visualisation of the processes taking place in this time span. For better visualisation, the R^3 cumulative heats up to one day are displayed in Fig. A2.

As shown in Fig. 3, the cumulative heat release for KCCs nearly reaches a plateau, indicating the primary pozzolanic reactions are largely complete within 7 days. In contrast, most other pozzolans, including FAs and some SCCs, exhibit pronounced slopes, suggesting ongoing reaction activity during this period. To further investigate these trends, a second R^3 campaign was conducted for selected SCMs, extending measurements to 14 days at 40 °C. The extended data, presented in Fig. 4 confirm the prolonged reactivity of these materials, with numerical values provided in Table 5 for detailed analysis.

The peak observed in the R^3 heat flow curves for all SCMs (see Fig. 4a and Fig. A1) are attributed to the formation of C–A–S–H gels, ettringite, and carboaluminate phases resulting from pozzolanic reactions [56]. It can be seen that these peaks have a large variability in their integrated areas which deserves discussion. The intense peak of KCC5 (given as an example of all KCC materials) is due to the fast intrinsic kinetics of the pozzolanic reaction of MK, in spite of its relatively low SSA value of 4 m^2 g^{-1}, see Table 4. All natural pozzolans and fly ashes have very slow pozzolanic intrinsic kinetics and this is evidenced as very small peaks. Conversely, Ref1-SCC and SF1 show relatively intense peaks. This large reactivity during the first day (at 40 °C) is justified because the very large SSA of Ref1-SCC and the small particle sizes of SF1. These features, large SSA and small particle sizes, are known to enhance the kinetics of the hydration reactions in general and the pozzolanic reaction(s) in particular. Two additional observations deserve attention. Firstly, SF2 has a similar SSA and amorphous content than SF1 but the intensity of this peak is significantly smaller. We speculate that the origin of this behaviour is its high iron content which is known to delay C-A-S-H formation. Secondly, Ref2-SCC has a smaller peak than Ref1-SCC. This is very likely due to its smaller SSA, 9 m^2 g^{-1}, see Table 4. In a nutshell, the four most important parameters to understand/justify the fast kinetics of pozzolanic materials are: (i) nature of the reactive phase (i.e. MK having the fastest intrinsic kinetics), (ii) the amount of reactive phase within the commercial SCM, (iii) the SSA (the highest the better but it increases the water demand), and (iv) the small particle size (the lowest the better).

3.4. *Pozzolanic reactivity of SCMs measured using the R^3 test at 40 °C – bound water*

ASTM C1897 also specifies the procedure for measuring the BW at 40 °C. The values obtained after seven days are presented in Table 5. As will be discussed below, the SAI at 28 days shows a stronger correlation with heat released at early ages. Consequently, BW measurements were also performed after maintaining the R^3 pastes at 40 °C for just one day, also shown in Table 5.

3.5. *Pozzolanic reactivity of SCMs measured using the modified SAI test at 20 °C*

As detailed in the experimental section, the first series with 80/20 blends was prepared with a constant water-to-binder (w/b) ratio of 0.50, i.e. not 0.485. Slump flow values were measured using the slump test, and PCE was added when needed to achieve similar flow values of 190 ± 30 mm, see Table 6. Compressive strengths were determined for the 22 SCMs at 28 days, and corresponding SAI values were derived. Additionally, a control mixture with inert quartz ($D_{V,50}$ = 15.5 μm) was tested to evaluate the filler effect. Most blends were also measured at 180 days, with results included in Table 6.

In a second campaign, 68/20/10/2 blend mortars were also tested,

Table 3
Mineralogical compositions including ACn of all SCMs used determined by RQPA and the internal standard method (KCCs and SCCs with Al_2O_3; NPs and FAs with ZnO). All data are expressed in weight percentage. The numbers in brackets are the associated standard deviations, as calculated by the Rietveld method.

Phases/ wt%	KCC1	KCC2	KCC3	KCC4	KCC5	KCC6	KCC7	Ref1-SCC	Ref2-SCC	SCC1	SCC2	SCC3	SF1	SF2	NP1	NP2	NP3	NP4	NP5	NP6	FA1	FA2
ACn	79	69	60	55	42	42	44	97	79	68	53	42	100	95	95	52	49	47	45	34	92	72
Qz	14.8(2)	31.1(1)	19.3(2)	14.5(2)	50.5(1)	63.2(1)	35.3(3)	3.5(3)	7.7(5)	2.6(4)	2.1(3)	–	–	–	–	6.4(2)	8.1(1)	3.4(2)	–	–	–	4.7(1)
Cristobalite	–	–	–	–	–	–	–	–	–	–	4.9(2)	–	–	–	–	–	–	–	–	–	–	–
Muscovite	–	–	13.7(3)	21.5(3)	–	3.5(2)	15.3(5)	–	–	15.0(1)	–	16.9(1)	–	–	–	–	–	4.1(4)	–	–	–	–
Microcline	–	–	6.2(3)	8.0(5)	6.3(2)	5.7(2)	–	–	5.0(5)	3.4(1)	2.1(1)	–	–	–	–	–	–	3.9(7)	–	–	–	–
Sanidine	–	–	–	–	–	–	–	–	–	1.4(1)	5.7(8)	12.2(7)	–	–	–	–	–	19.7(8)	–	–	–	–
Diopside	–	–	–	–	–	–	–	–	–	–	–	–	–	–	–	32.0(4)	29.4(3)	4.9(4)	43.9(3)	29.0(4)	–	–
Leucite	–	–	–	–	–	–	–	–	–	–	–	–	–	–	–	–	–	–	–	24.2(4)	–	–
Nepheline	–	–	–	–	–	–	–	–	–	–	–	–	–	–	–	–	–	–	–	4.1(2)	–	–
Fosterite	–	–	–	–	–	–	–	–	–	–	–	–	–	–	–	–	11.1(4)	–	11.3(3)	–	–	–
Albite	–	–	–	–	–	–	–	–	7.0(5)	1.4(1)	–	9(1)	–	–	–	3.2(4)	–	–	–	–	–	–
Andesine	–	–	–	–	–	–	–	–	–	–	–	19.9(1)	–	–	–	–	–	–	–	–	–	–
Anorthite	–	–	–	–	–	–	–	–	–	8.2(1)	30.1(5)	–	–	–	–	–	–	–	–	–	–	–
Analcyme	–	–	–	–	–	–	–	–	–	–	–	–	–	–	–	3.8(2)	–	16.9(3)	–	–	–	–
Mullite	–	–	–	–	–	–	–	–	–	–	–	–	–	–	–	–	–	–	–	–	3.4(4)	21.8(2)
Amphibole	–	–	–	–	–	–	–	–	–	–	2.1(5)	–	–	–	–	–	–	–	–	–	–	–
Fe_2O_3	4.4(2)	–	–	–	–	–	4.8(2)	–	–	–	–	–	–	–	–	–	–	–	–	4.7(2)	–	–
SiC	–	–	–	–	–	–	–	–	–	–	–	–	–	3.3(2)	–	–	–	–	–	–	–	–
Minors	2.1	0.3	1.0	0.7	1.0	0.1	0.5	–	1.0	2.2	–	–	–	2.1	5.0	2.4	2.2	–	5.0	3.8	4.7	1.7

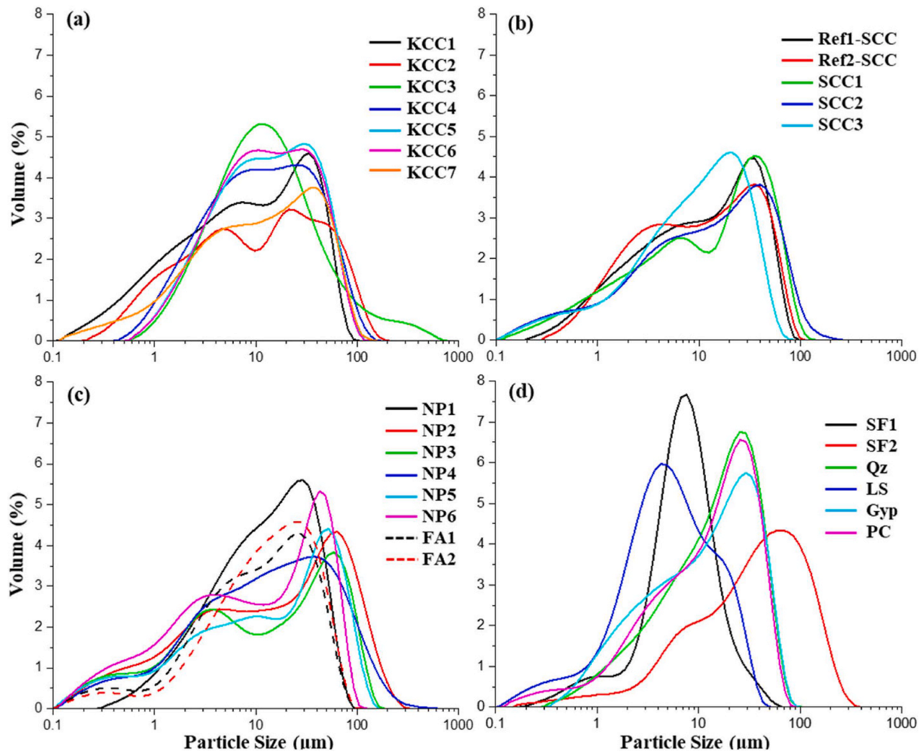

Fig. 1. Particle size distribution traces, displayed as relative volume percentage, for (a) KCCs, (b) SCCs, (c) NPs and FAs, and (d) references and other employed materials.

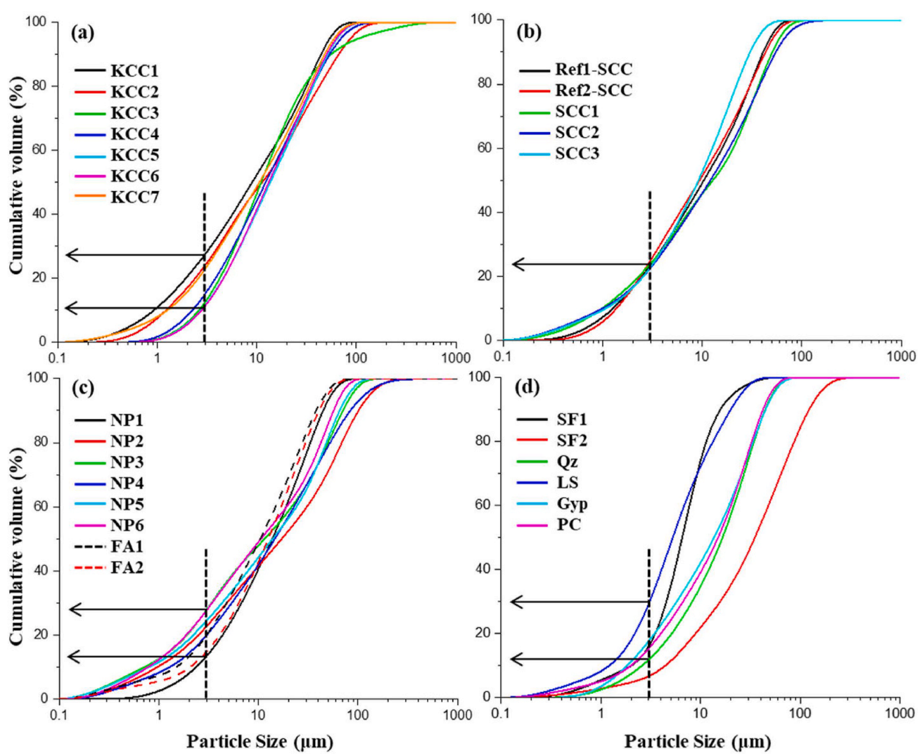

Fig. 2. Particle size distribution traces, displayed as cumulative volume, for (a) KCCs, (b) SCCs, (c) NPs and FAs, and (d) reference and other employed materials. The range of volume fractions with particle sizes smaller than 3 μm is highlighted by black arrows.

Table 4
Textural properties of SCMs and other materials used in this study.

	$D_{V,10}$ (μm)	$D_{V,50}$ (μm)	$D_{V,90}$ (μm)	$V_{<3.0\ \mu m}$ (%)	BET (m^2/g)	Density (g/cm^3)
KCC1[a]	0.9	8.4	41.4	27.0	27.2	2.71
KCC2[b]	1.2	11.3	66.4	24.6	25.4	2.64
KCC3[c]	2.8	11.8	58.9	12.0	10.0	2.63
KCC4[c]	2.1	11.8	51.6	14.5	7.6	2.63
KCC5[c]	2.5	12.0	47.0	11.0	4.0	2.63
KCC6[c]	2.7	12.3	47.8	10.8	3.2	2.61
KCC7[a]	1.5	12.0	54.6	23.5	4.5	2.71
Ref1-SCC[d]	0.7	10.6	50.4	24.1	131.4	2.57
Ref2-SCC[d]	0.9	11.1	63.0	25.7	9.1	2.51
SCC1[d]	1.1	14.5	57.4	24.5	51.9	2.78
SCC2[d]	1.1	13.7	62.3	23.2	11.4	2.60
SCC3[d]	1.2	10.4	34.3	23.5	18.1	2.64
SF1	–	–	–	–	22.0	2.28
SF2	–	–	–	–	25.8	2.36
NP1[e]	2.2	12.8	41.0	13.0	9.3	2.28
NP2[d]	0.9	16.0	95.0	22.3	24.0	2.80
NP3[d]	0.8	13.1	80.0	28.6	30.9	3.18
NP4[d]	1.2	13.7	79.0	19.6	10.4	2.55
NP5[d]	0.9	15.7	74.3	25.0	9.7	3.01
NP6[d]	0.7	10.0	53.0	27.3	18.1	2.81
FA1[d]	1.7	11.8	43.2	20.6	3.1	2.40
FA2[d]	2.3	14.3	46.0	15.3	1.8	2.32
Qz[c]	2.4	15.5	41.6	11.5	0.9	2.67
LS[e]	1.1	4.9	18.8	28.3	2.0	2.73
Gyp[f]	1.7	12.8	41.9	17.2	6.3	2.38
PC[g]	1.9	14.0	40.0	14.9	1.4	3.11

Refractive index (RI) and absorption index (AI): a: (RI: 1.55, AI: 0.1) b: (RI: 1.55, AI: 0.05) c: (RI: 1.55, AI: 0.01) d: (RI: 1.53, AI: 0.1) e: (RI: 1.66, AI: 0.01) f: (RI: 1.53, AI: 0.01) g: (RI = 1.68, AI = 0.1). These values are used in the calculation of light scattering for non-spherical particles using the MIE method.

see Table 7. In this series, the SCM content was maintained at 20 %, while 12 % of PC was replaced with 10 % limestone and 2 % gypsum.

4. Discussion

4.1. Elemental and mineralogical compositions of the SCMs

Firstly, kaolinitic and smectitic calcined clays exhibit some compositional relationships, particularly in their SiO_2 and Al_2O_3 contents. For the studied calcined clays, the Al_2O_3 content ranged from 16 to 34 % for kaolinitic materials and from 9 to 20 % for smectitic ones. While lower Al_2O_3 content in smectites was expected, the actual values depend on the presence of secondary phases, such as muscovite and feldspars. Moreover, this work characterized four montmorillonites (dioctahedral, with mainly Al^{3+} in the octahedral sheet) and one saponite (i.e. SCC1, trioctahedral, with predominantly Mg^{2+} in the octahedral sheet). Therefore, while 'Al_2O_3 content' can serve as a descriptor for SCMs, it should be monitored carefully, as it does not necessarily correlate with

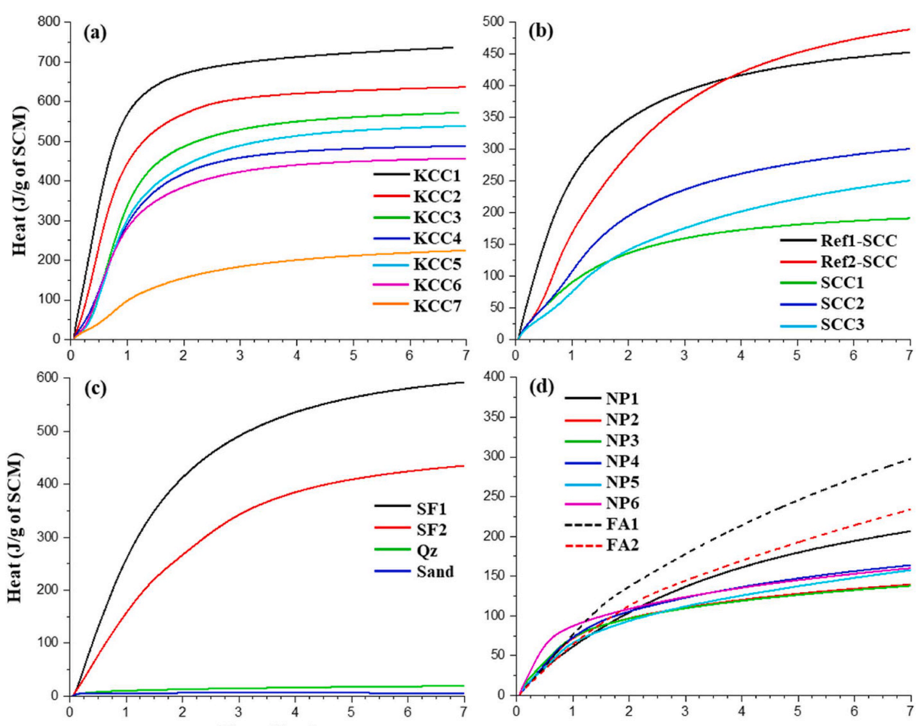

Fig. 3. Cumulative heat curves for R^3 mixtures over seven days. (a) KCCs, (b) SCCs, (c) SFs and inert materials, and (d) NPs and FAs.

Table 5
R^3 test results, including bound water (g/100 g of dried paste) at 1 and 7 days, and cumulative heat release (J/g of SCM) at the specified times. Italicised values represent heat release from a second set of measurements extended to 14 days. The variation (%) between 7 and 14 days is also provided.

	Bound water		Heat released					Δ heat (%)
	BW 1 d	BW 7 d	1/2 d	1 d	3 d	7 d	14 d	*(7–14 d)*
KCC1	8.9	12.1	342	577	698	737	–	–
KCC2	8.7	10.3	236	445	608	637	–	–
KCC3	7.5	9.8	122	342	530	572	–	–
KCC4	6.3	9.4	125	291	459	488	–	–
KCC5	6.4	9.7	110/*89*	302/*291*	490/*490*	539/*542*	-/*554*	*2*
KCC6	6.3	8.0	121	285	423	457	–	–
KCC7	3.6	5.4	42	98	184	225	–	–
Ref1-SCC	5.6	8.1	148/*138*	253/*268*	391/*390*	452/*439*	-/*471*	*7*
Ref2-SCC	4.6	8.1	66/*61*	166/*149*	372/*336*	489/*449*	-/*497*	*11*
SCC1	2.0	4.2	51/*50*	90/*91*	160/*159*	191/*190*	-/*199*	*5*
SCC2	3.3	5.1	52/*52*	107/*109*	236/*241*	301/*296*	-/*324*	*9*
SCC3	3.4	5.8	38/*37*	75/*75*	176/*177*	251/*253*	-/*302*	*19*
SF1	5.8	8.9	128/*138*	258/*267*	491/*500*	593/*603*	-/*638*	*6*
SF2	4.3	6.5	*77/78*	164/*153*	342/*342*	435/*457*	-/*499*	*9*
NP1	3.6	5.7	34/*37*	62/*63*	137/*133*	207/*197*	-/*240*	*22*
NP2	3.5	5.0	37/*43*	75/*76*	110/*115*	139/*140*	-/*154*	*10*
NP3	2.8	4.8	42/*65*	73/*92*	110/*123*	137/*150*	-/*175*	*17*
NP4	3.1	5.2	38/*38*	73/*71*	123/*126*	164/*167*	-/*194*	*16*
NP5	2.9	4.2	35/*41*	67/*68*	112/*103*	158/*128*	-/*153*	*20*
NP6	3.3	5.1	62/*60*	87/*92*	124/*129*	160/*163*	-/*191*	*17*
FA1	2.8	5.8	36/*34*	77/*68*	178/*177*	297/*299*	-/*412*	*38*
FA2	2.5	5.4	32/*31*	64/*60*	144/*153*	233/*251*	-/*350*	*39*
Qz	1.6	1.6	8	10	15	19	–	–
Sand	1.4	1.4	5	5	6	5	–	–

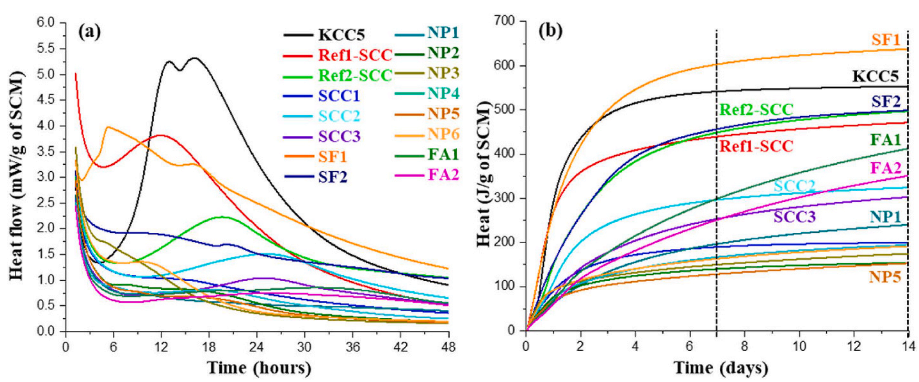

Fig. 4. Isothermal calorimetry results for R^3 pastes of selected SCMs, extended to 14 days. (a) Heat flow curves. (b) Cumulative heat release traces.

pozzolanic performance. Even among montmorillonite-based smectitic clays, the montmorillonite phase may feature different interlayer cations, such as calcium (Ca-Mnt) or sodium (Na-Mnt), among others. The corresponding meta-smectites are therefore expected to exhibit varying solubilities during early reaction stages.

Secondly, the amorphous content is a descriptor to be monitored as there is a qualitative agreement between the amount of amorphous fraction, see Table 3 and the pozzolanic features, see Table 5. However, not all amorphous phases exhibit pozzolanic activity, and their reaction kinetics can vary significantly. As a result, a quantitative correlation between the amorphous content of SCMs and their pozzolanic performance at a given age cannot be expected.

The potassium content should also be considered, as it may influence the kinetics of cement hydration [69]. However, when potassium is primarily incorporated in crystalline phases such as muscovite or feldspars (e.g., microcline), their contribution to pozzolanic reactivity is generally negligible [70,71]. Therefore, in addition to the overall potassium content determined by XRF, the amount of potassium dissolved under relevant conditions is important for K-rich SCMs. However, pore solution measurements were not within the scope of the present investigations.

Therefore, while elemental and mineralogical analyses of potential SCMs are useful for initial screening, as of today, they cannot replace the pozzolanic tests.

4.2. Textural properties of the SCMs

On the one hand, there is consensus that smaller average particle sizes of SCMs generally lead to higher pozzolanic hydration rates and improved final hydration performance. However, for multicomponent SCMs, it is often very difficult, or even impossible, to determine the average particle size of the active phase (i.e. the amorphous components in many cases). Moreover, very fine particle sizes can result in excessive energy requirements during milling and also relatively high-water demand. A large volume of smaller particles may explain the enhanced early-age reactivity of certain SCMs. To monitor this, Table 4 reports the volume percentage for particles smaller than 3 μm, for all SCMs. This threshold, i.e. 3 μm, was subjectively chosen based on recent findings regarding the change in alite hydration rate with particle size [72]. It is important to recognise that the optimal particle size is SCM-dependent and may even vary with application. In this study, we have adopted the strategy to mill, when possible, all SCMs to $D_{V,50}$≈12 μm. This approach reflects two key decisions. Firstly, achieving similar particle sizes for all SCMs ensures robust comparisons in this general study.

Table 6
Mortar study results for the 80/20 series, including the amount of PCE required to achieve an initial slump of 190 ± 30 mm and the corresponding slump values. Mechanical (compressive) strengths for the blends at 28 and 180 days.

	PCE wt%	Slump/mm	28d-M.S./MPa	28d-SAI/%	180d-M.S./MPa	180d-SAI/%
KCC1	0.30	189(1)	66(2)	111	78(2)	104
KCC2	0.40	164(1)	70(2)	118	73(1)	97
KCC3	0.40	173(1)	58(2)	98	66(2)	88
KCC4	0.50	201(1)	60(1)	102	75(2)	100
KCC5	0.20	185(1)	61(1)	103	72(1)	96
KCC6	0.15	197(1)	60(1)	101	72(2)	96
KCC7	–	179(1)	59(1)	99	–	–
Ref1-SCC[a]	–	–	65(1)	107	–	–
Ref2-SCC[a]	–	–	57(1)	93	–	–
SCC1	0.40	175(3)	58(1)	98	67(1)	89
SCC2	0.30	208(1)	59(1)	99	73(4)	97
SCC3	0.20	187(1)	55(1)	93	67(1)	89
SF1	0.40	187(1)	66(2)	111	80(1)	107
SF2	0.40	182(1)	57(2)	97	–	–
NP1[b]	0.60	168(1)	49.5(4)	83	67(1)	89
NP2	–	177(1)	53(1)	89	65(1)	87
NP3	–	179(3)	54(1)	91	63(2)	84
NP4	–	175(1)	51(1)	86	62(1)	83
NP5	–	188(2)	53(1)	89	–	–
NP6	–	194(1)	56(1)	95	70(1)	93
FA1	–	189(4)	50(2)	84	76(5)	101
FA2	–	222(3)	51.2(2)	86	–	–
Qz	–	180(1)	53(1)	89	62(1)	83
PC	–	189(1)	59(1)	–	75(1)	–

[a] The Ref1-SCC and Ref2-SCC mortars were tested using 30 × 30 × 30 mm cubes. No slump test was performed due to the limited quantity of material available.
[b] The mortar prepared with NP1, without the addition of PCE, exhibited an initial slump of 143(1) mm and achieved a compressive strength of 49(1) MPa at 28 days.

Table 7
Mortar study results for the 68/20/10/2 series, including the amount of PCE required to achieve an initial slump of 190 ± 30 mm and the corresponding slump values.

	PCE wt%	Slump/mm	28d-M.S./MPa	28d-SAI/%
KCC1	0.50	207(1)	62(2)	105
KCC3	0.50	176(1)	54(1)	91
KCC4	0.35	177(1)	55(1)	93
KCC5	0.20	208(1)	54(1)	91
KCC6	0.15	189(1)	53(1)	89
KCC7	–	183(1)	46(2)	78
SCC1	0.60	186(1)	51(1)	86
SCC2	0.50	215(1)	56(1)	94
SCC3	0.40	255(6)	50(1)	84
SF1	0.50	185(1)	63(1)	106
SF2	0.40	183(1)	51(1)	86
NP1	0.60	172(2)	43(1)	73
NP2	–	184(5)	43(1)	72
NP3	–	184(1)	45(1)	77
NP4	–	172(1)	43(1)	72
NP5	–	189(2)	43(1)	73
NP6	–	187(4)	47(1)	80
FA1	–	188(3)	45(1)	76
FA2	–	202(1)	43(1)	73
Qz	–	190(1)	41(1)	69

Secondly, the target size of ≈12 µm was selected to be slightly smaller than the particle size of the PC used, which was 14 µm, see Table 4. It is acknowledged that determining the optimal particle size for specific SCMs, here referred to as 'smart SCM milling', remains an active R&D field.

On the other hand, specific surface area is another important texture-related parameter. In principle, the higher the SSA of an SCM, the greater its pozzolanic hydration rate at early ages. As mentioned above, SSA is a compound function of all components present. However, the critical value of interest is the SSA of the active component(s) within the SCM, which is extremely difficult to measure in multicomponent materials. SSA can decrease during the thermal activation step but in many cases it is not significantly affected by the milling process, unless mechanochemical activation procedures are employed [73]. In this study, the SSA of the SCMs was always monitored to better understand their pozzolanic behaviour, but it was not a target.

For KCCs, there is a clear trend between MK content and SSA for amounts exceeding ≈40 wt%, see Table 4. For calcined clays with MK contents below this threshold, the nature of the secondary phases can dominate the measured SSA values. For SCCs, SSA exhibits significant variation depending on the sample, see Table 4, as expected due to the layered and exfoliating nature of the pristine materials. For NPs, which

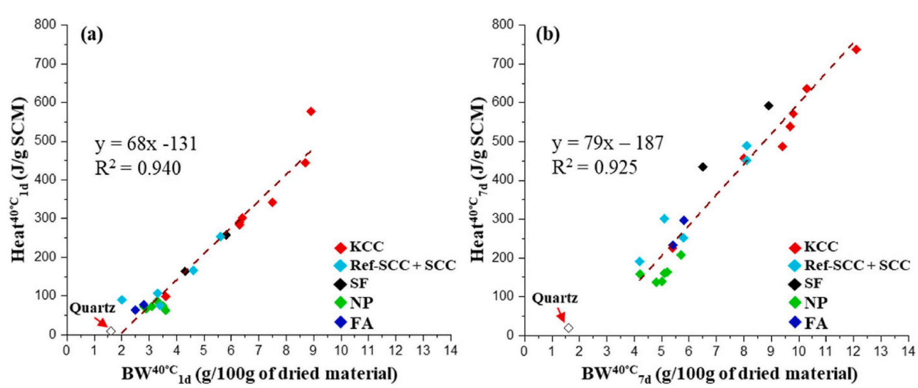

Fig. 5. Linear correlation between cumulative heat release and bound water (R^3 test), for all studied SCMs: (a) results at 1 day, and (b) results at 7 days.

typically have slower pozzolanic reaction rates, achieving low particle sizes and high SSA is critical for enhancing reactivity. As shown in Table 4, the SSA of the six studied materials varies by more than 70 %, despite their average particle sizes differing by less than 37 %. High SSA is beneficial for early age pozzolanic reactivity, as will be demonstrated below.

Finally, the density of all the SCMs was measured for precautionary reasons. However, density values are not yet a reliable proxy for pozzolanic performance, nor do they show a clear correlation with pozzolanic activity.

4.3. R^3 test results

Fig. 5 shows the correlation between cumulative heat release and bound water (BW) for all studied SCMs. These results confirm and expand upon findings from a recent RILEM publication [57], which reported a linear correlation between heat and BW at seven days (R^2 = 0.87, slope = 71 J/g, intercept = −157 J/g). In this study, the correlation is slightly improved, with an (R^2 = 0.93, slope = 79 J/g, intercept = −187 J/g), see Fig. 5b. Additionally, this work extends the analysis to early-age conditions, with measurements taken at 1 day. The resulting correlation was even stronger (R^2 = 0.94, slope = 68 J/g, intercept = −131 J/g), see Fig. 5a. These results suggest that both approaches, heat release and BW, can be used interchangeably to predict the pozzolanic reactivity of an SCM. However, while BW measurements are more cost-effective, isothermal calorimetry provides continuous data, offering better insight into kinetic behaviour. Furthermore, the correlation between cumulative heat and relative compressive strength is slightly stronger, as discussed below.

A detailed inspection of Fig. 5 raises questions about whether the correlation is consistent, within the margin of error, for KCCs (red diamonds) compared to other SCMs. Since KCCs behave differently for the R^3-SAI correlation, see below; a secondary analysis was performed, with separate fits for KCCs and other SCMs, see Fig. A3. The results indicate that for non-KCC SCMs, the slope changes significantly over time (1 day: slope = 56 J/g; 7 days: slope = 94 J/g). Conversely, the slope for KCCs remains relatively stable (1 day: slope = 80 J/g; 7 days: slope = 75 J/g). These preliminary observations highlight the need for further research to fully establish the implications of these findings and their potential consequences.

The discussion now centres on the cumulative heat released at 40 °C, representing overall pozzolanic performance, see Fig. 3, and its evolution during the first day, indicative of the early-age pozzolanic reaction rate, see Fig. A2. It is important to note that the early-age pozzolanic reaction rate at 40 °C, as measured by the R^3 test at 1 day, may correspond to pozzolanic activity at approximately 28 days under room temperature conditions. This study also seeks to establish a stronger connection between R^3 results at 40 °C and compressive strength results at 20 °C.

For the KCC series, heat release varies smoothly and the obtained values align closely with those expected based on their estimated MK contents. Three independent studies on high-purity MK samples reported cumulative heat releases at seven days of 1150, 1085 and 1030 J/g of in Refs. [27,49,74], respectively. Pure MK consists of 54 % of SiO_2 and 46 % of Al_2O_3. The thermodynamically calculated heat release for the complete reaction of SiO_2 to form C-S-H with a Ca/Si ratio of 1.70 is 769 J/g (maximum/theoretical value) [75]. Similarly, the heat release for Al_2O_3 reacting with $Ca(OH)_2$ in the presence of excess carbonates to produce monocarboaluminate is 1402 J/g [75]. Using a simplified calculation, $769 \times 0.54 + 1402 \times 0.46 = 1060$ J/g, the estimated value aligns well with experimental results, given the implicit approximations. Therefore, pure MK can be considered to release 1100 J/g after full reaction. Based on this, a MK content of 40 % would yield approximately 440 J/g of cumulative heat. This agrees with the values observed for KCC6 and KCC4, see Fig. 3a. For KCC4, which has a MK content of ≈20 %, the heat release of 220 J/g matches expectations. KCC5, however, released approximately 20 % more heat than expected, as the raw clay has an estimated kaolinite content of ≈40 %. This discrepancy could stem from inaccuracies in kaolinite content determination and/or contributions from the amorphous fraction to the pozzolanic reaction.

For the SCC series, the discussion of heat release requires further elaboration due to the absence of a model sample and the diversity of smectite compositions. On the one hand, for the reference smectites, Ref1-SCC (Ca-Montmorillonite, ≈93 %) released ≈450 J/g at seven days, while Ref2-SCC (Na-Montmorillonite, ≈75 %) released ≈490 J/g at seven days, see Fig. 3b. The relatively lower Al_2O_3 content in these samples limits the significant formation of carboaluminates, resulting in lower heat release values overall. Moreover, it is reasonable to conclude that Na-Montmorillonite intrinsically releases more heat (i.e. it is more reactive) than Ca-Montmorillonite. However, the Ca-Montmorillonite studied here exhibits much higher pozzolanic activity at early ages, Fig. A2b, likely due to its significantly higher SSA, 131 m^2/g, compared to 9 m^2/g for the Na-Montmorillonite sample. On the other hand, for the commercial smectite clays, SCC1 (saponite, ≈80 %) released only ≈200 J/g at seven days. This relatively low value is likely due to the absence of reactive aluminium in the meta-smectite phase. Nevertheless, its early-age pozzolanic reactivity, Fig. A2b, is comparable to that of the meta-montmorillonites, likely owing to its high SSA of 52 m^2/g. SCC2 and SCC3 (Na-Mnt) released ≈300 J/g and ≈250 J/g, respectively. These values are slightly lower than expected based on their Na-Mnt contents (74 % and 53 %, respectively). However, the agreement is reasonably good considering the challenges in accurately determining smectite content and the inherent variability in the element compositions of natural clays.

Concerning the studied silica fumes, SF1, with ≈100 % amorphous content, released ≈600 J/g at seven days, see Fig. 3c. Conversely, SF2, with ≈95 % amorphous content, released ≈440 J/g. The lower heat release for SF2 is attributed to its relatively high Fe_2O_3 content (4.6 %), which may partially inhibit the pozzolanic reaction, as previously reported [76]. These values align well with those previously reported for three commercial SFs, which ranged from 520 to 630 J/g [57]. Notably, the Fe_2O_3 contents of these SFs were smaller than 3 %. An anomalously low value of 350 J/g has been reported for a SF [77], but this discrepancy could be due to experimental issues and/or variability among commercial products. As discussed above, the theoretical maximum value (representing a 100 % degree of reaction) is approximately 770 J/g [75].

For the NPs series, see Fig. 3d, the heat release values at seven days ranged from 137 to 207 J/g. These are low values, and for two samples, NP2 and NP3, the heat release falls below the 160 J/g threshold specified by the ASTM C1897 standard for classifying a material as pozzolanically reactive at a 90 % confidence level. However, this strict limit excludes slow-reacting materials that contribute significantly to long-term strength development. Using the 66 % confidence level threshold recommended by RILEM (i.e. a heat of 98 J/g) [57], all commercial natural pozzolans tested here can be classified as pozzolanically active. The measured heat release values compare relatively well with previously reported data. For example, in Ref. [60], 7-day heat release values for three volcanic ashes ranged from 180 to 270 J/g, with the highest value (270 J/g) corresponding to a sample with a relatively small $D_{V,50}$ of 6.3 μm. Another study [49] reported 7-day heat release values of 263 J/g and 200 J/g for pumicite and tuff, respectively. In this study, five NPs are classified as volcanic ashes, while NP4 is trass-like, i.e. zeolitised. NP1, with the highest amorphous content (≈95 %), released the greatest heat at seven days (207 J/g). However, its pozzolanic reaction rate at early ages is slow, see Fig. A2d. This could be due to its relatively low SSA of 9 m^2/g and its low fraction of small particles, $V_{<3\mu m}$≈13 %, see Table 4. In contrast, NP6 exhibited the fastest pozzolanic reaction rate at early ages, Fig. A2d, despite having only 34 % amorphous content. This behaviour can be explained by three factors: (i) a relatively high SSA of 18 m^2/g, (ii) a large fraction of fine particles, $V_{<3\mu m}$≈27 %, see Table 4; and (iii) its classification as a basic rock with a high K_2O

Table 8
Square of the correlation coefficient values (i.e. R^2) for the linear regressions between R^3 test results (Bound water and Heat released) and relative compressive strength across different curing ages for the two investigated blends. In italics, the R^2 values of the non-kaolinitic SCMs, named as other SCMs. The R^2 values higher than 0.75 are highlighted in bold, as they indicate good correlations.

Relative compressive strength	Bound water		Heat released			
	(KCCs/*Other SCMs*)		(KCCs/*Other SCMs*)			
	1 d	7 d	1/2 d	1 d	3 d	7 d
28 days $_{80/20\ series}$	0.509/*0.512*	0.338/*0.399*	0.611/***0.805***	0.511/***0.778***	0.433/*0.646*	0.412/*0.499*
180 days $_{80/20\ series}$	0.067/*0.362*	0.227/*0.540*	0.422/*0.505*	0.277/*0.563*	0.169/*0.677*	0.148/***0.768***
28 days $_{68/20/10/2\ series}$	**0.900**/*0.415*	**0.940**/*0.440*	**0.862**/*0.727*	**0.961**/***0.743***	**0.944**/***0.759***	**0.931**/*0.663*

content of 6.5 %. Overall, the heat release patterns align with our understanding that amorphous content governs long-term performance, while texture properties (e.g., fineness and SSA) influence early-age pozzolanic reactivity. The exception is NP3, which deviates from this pattern. Despite its high fineness and significant amorphous content (≈50 %), NP3 released less heat and reacted at a slower rate than anticipated. Further research is required to fully understand the pozzolanic behaviour of this sample.

Two Class-F FAs were included in this study for comparison purposes, as the pozzolanic behaviour of FA is well-documented [46,47,78]. The cumulative heat release at seven days for the two FA samples studied here was 297 J/g for FA1 and 233 J/g for FA2. These values align relatively well with those reported in Ref. [79], where two fly ashes with $D_{V,50}$ values of 12 μm and 17 μm, and amorphous contents of 83 % and 75 %, exhibited cumulative heat releases of 280 J/g and 262 J/g, respectively. A broader range of cumulative heat values from 150 to 350 J/g was reported for eight fly ashes in Ref. [57]. The amorphous contents of FA1 and FA2 are ≈92 and ≈ 72 %, respectively, with their finesses, measured as $V_{<3μm}$, are 21 and 15 %, respectively. The higher amorphous content and finesse of FA1 fully justify its greater heat release, see Fig. 3d. As expected, the pozzolanic reaction rates of FAs are slow, see Fig. A2d.

Inert materials, i.e. quartz and standard sand, were effectively screened by the R^3 test. The cumulative heat release at seven days was 19 J/g for quartz and 5 J/g for sand, see Fig. 3c.

Finally, as the cumulative heat release had not stagnated at seven days for some slow-reacting SCMs, see Fig. 3, a second set of measurements was carried out but extended up to 14 days, see Fig. 4b. Table 5 reports the cumulative heats at 14 days and chiefly, the relative variation between 7 and 14 days. KCC5, was chosen to represent the kaolinitic calcined clays due to its intermediate kaolinite content, and its variation was minimal (2 %). Similarly, SFs, which have a fast pozzolanic reaction rate, showed a small variation from 6 to 9 %. For calcined smectitic clays, the variation was larger, ranging from 5 % for SCC1 to 19 % for SCC3. The greatest variation was observed in FAs, with approximately 40 % of the cumulative heat being released during the 7–14 days period, see Fig. 4b, indicating that 7 days is insufficient to capture the full pozzolanic potential of FAs. To end this subsection, the NPs behaviour is briefly discussed. The relative variations ranged from 10 % for NP2 to 22 % for NP1. NP1 exhibited the largest heat release in the 7–14 day period, likely due to its low fraction of small particles, i.e. $V_{<3μm}$ is only 13 %, see Table 4.

4.4. Modified SAI results

Despite maintaining a constant w/b ratio, and using the recommended 20 % replacement, the quartz sample, demonstrated above to be inert, met the SAI test requirement of 75 % at 28 days, as established by ASTM C311-02, see Table 6. This has been extensively reported and discussed [80,81], and it is attributed to the filler effect. It has been proposed to raise the SAI strength requirement [81], even increasing it to 85 % would still result in a false positive in this case. Moreover, raising the threshold would result in failures for slow-reacting materials, such as NPs and FAs. To address this, compressive strength measurements at 28 days should be conducted in mortars with lower PC contents, as previously discussed [48,49,55,57,79]. Accordingly, a second series of mortars were prepared with 68 % PC, the 68/20/10/2 blend series, see Table 7. In this case, the filler contribution is minimised, and the mortar containing quartz gave the lowest SAI value at 28 days, i.e. 69 %. By contrast, all eight slow-reacting commercial pozzolans (i.e., NPs and FAs) exhibited higher SAI values, ranging from 72 % to 80 %, see Table 7.

For the 80/20 blends, KCCs were the most reactive SCMs at 28 days, with SAI values ranging from 98 to 118 %. SCCs were also highly reactive, achieving SAI_{28d} values between 93 and 107 %. Conversely, and as expected, NPs and FA were the least reactive SCMs at 28 days, with SAI value ranging from 83 to 95 %. Notably, NP6 achieved a relatively high SAI value of 95 %, which is unusual for a natural pozzolan. This behaviour can be attributed to its high early-age reactivity, as demonstrated by the R^3 test, see Fig. A2d, and discussed above.

For this series, a second campaign of SAI measurements was conducted at 180 days. Notably, the SAI_{180d} values for all KCCs were lower than their corresponding values at 28 days. This indicates that KCCs are highly reactive during the first weeks but their reactivity diminishes as their potential becomes exhausted. Consequently, the compressive strength of the blends cannot match the continued strength increase of the PC employed. SCCs exhibited a similar pattern, with SAI_{180d} values being smaller than SAI_{28d} ones. Conversely, and as widely reported, FA1 showed a very large increase in SAI value, from 84 % at 28 days to 101 % at 180 days. SF1 performed consistently well at both ages, with SAI values of ≈110 %. The long-term behaviour of NPs was more variable. NP1, which has the highest amorphous content, showed an increase from 83 % at 28 days to 89 % at 180 days. However, NP3, with ≈50 % of amorphous content and the largest fraction of fine particles, experienced a decrease from 91 % to 84 %. These observations suggest that significant quantities of the active component within slow-reacting SCMs are necessary to sustain increasing SAI values beyond the first months of hydration.

Concerning the 68/20/10/2 blend series, the SAI_{28d} values for KCCs varied smoothly, ranging from 105 % for the calcined clay with the highest MK content to 78 % for the clay with the lowest MK content. A similarly smooth variation was observed for SCCs, with values ranging from 94 % to 85 %. As anticipated, NPs and FAs displayed lower values, ranging from 80 % to 72 %. Finally, SFs performed exceptionally well, with SF1 achieving 106 %.

4.5. General correlation between R^3 results and modified SAI outputs

Previous studies have reported correlations between relative compressive strength (RCS) and R^3 test results. In RILEM publication [57], a 30 % SCM replacement level was selected for five SCM families (SFs where left out as their replacement level was 10 %). Although the w/b ratio was not explicitly given, 0.50 is deduced because it followed EN 196-1 standard. Two clear trends were observed when fitting RCS at 28 days and 20 °C versus the $Heat^{4^\circ C}_{7d}$. Kaolinitic calcined clays produced a fit with $R^2 = 0.84$, slope = 0.047 g/J, and intercept = −34. In contrast, the rest of the investigated SCMs yielded a fit with $R^2 = 0.87$, slope = 0.095 g/J, and intercept = −39. It should be noted that smectitic

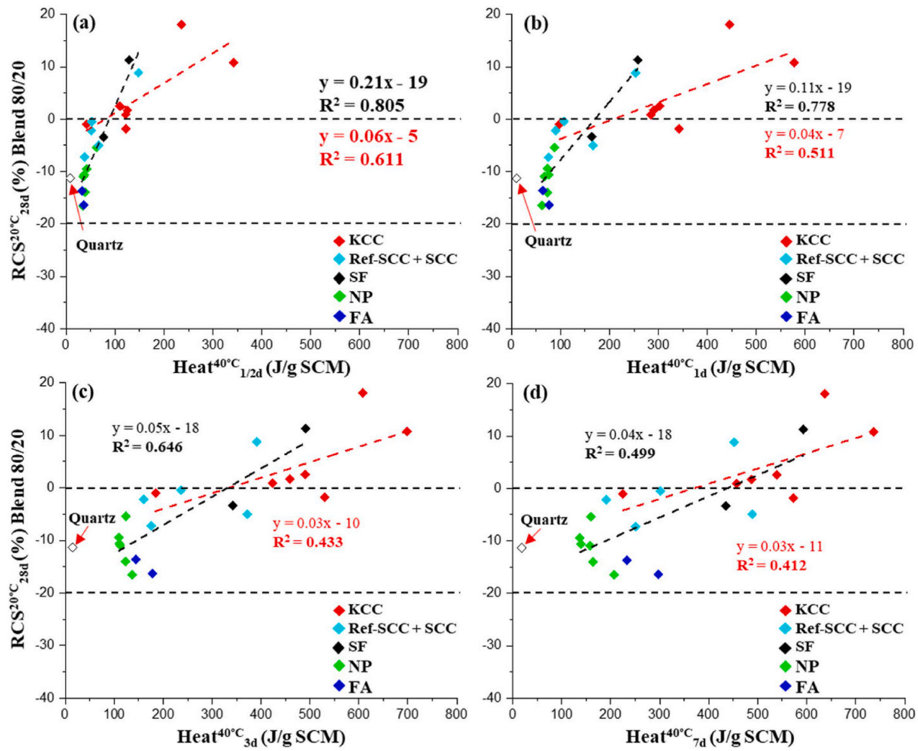

Fig. 6. Linear correlation plots of the relative compressive strength (RCS) at 20 °C for the 80/20 blends versus cumulative heat release of the corresponding SCMs at the given times. (a) 1/2 day, (b) 1 day, (c) 3 days, and (d) 7 days. Two distinct trends are observed: kaolinitic calcined clays (red fits), all other pozzolans (black fits). The horizontal dashed lines highlight the PC replacement values of 0 and 20 %. (For interpretation of the references to colour in this figure legend, the reader is referred to the Web version of this article.)

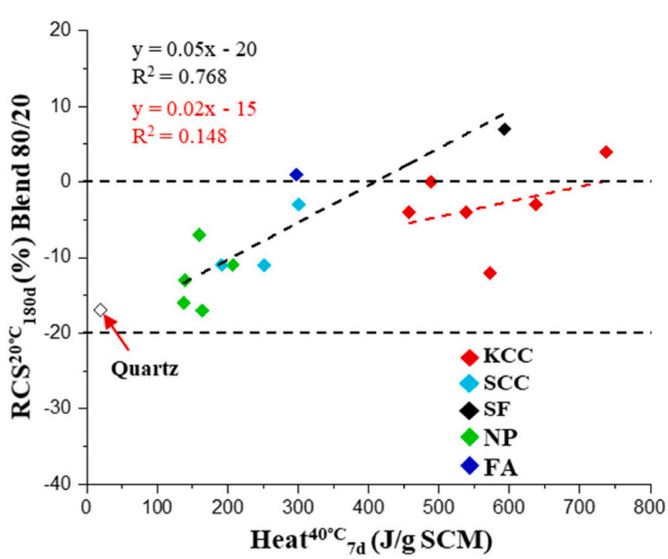

Fig. 7. Linear correlation plot of the relative compressive strength at 20 °C and 180 days versus cumulative heat release at 7 days for the 80/20 blends. All details as in Fig. 6.

calcined clays were not included in this study. In Ref. [79], 25 % SCM replacement level was used with a fixed w/b ratio of 0.485. Only one trend was observed, as the study investigated just two calcined clays (pure and impure metakaolin). The linear fit of $\mathrm{SAI}^{20\,^\circ\mathrm{C}}_{28d}$ versus $\mathrm{Heat}^{40\,^\circ\mathrm{C}}_{7d}$ gave $R^2 = 0.79$ and slope = 0.055 g/J. Finally, in another RILEM publication [48], a 30 % SCM replacement level was adopted, with a w/b ratio of 0.50 inferred from adherence to the EN 196-1 standard. $\mathrm{SAI}^{20\,^\circ\mathrm{C}}$ values at 7, 28 and 90 days were fitted to various pozzolanic performance descriptors, including $\mathrm{BW}^{40\,^\circ\mathrm{C}}_{7d}$ and $\mathrm{Heat}^{40\,^\circ\mathrm{C}}_{1/2,1,3,7d}$, consumed portlandite, and chemical shrinkage. The results, summarised in Table 4 of [48], demonstrated that Heat consistently provided better fits than BW. $\mathrm{SAI}^{20\,^\circ\mathrm{C}}_{7d}$ correlated better with Heats at ½ and 1 day, $R^2 = 0.95$. Similarly, the $\mathrm{SAI}^{20\,^\circ\mathrm{C}}_{28d}$ matched best with Heat at 7 days, $R^2 = 0.94$. Interestingly, $\mathrm{SAI}^{20\,^\circ\mathrm{C}}_{90d}$ did not correlate with $\mathrm{Heat}^{40\,^\circ\mathrm{C}}$ at any age, the best R^2 value was only 0.63, observed for $\mathrm{Heat}^{40\,^\circ\mathrm{C}}_{7d}$.

Here, we have complemented and extended previous works with several innovations to identify the conditions under which the best correlations occur: (i) the w/b ratio was fixed at 0.50, with PCE added only when strictly necessary; (ii) bound water content, as measured by the R^3 methodology at 40 °C, was also assessed at 1 day, as it may better reflect the 28 days pozzolanic reactivity of blends at room temperature; (iii) for the 80/20 blends, SAI values were measured at both 28 and 180 days; and most importantly (iv) SAI values for a new blend family, with 68 wt% PC, 20 wt% SCM, 10 wt% limestone, and 2 wt% gypsum were measured at 28 days.

Table 8 summarises the R^2 values obtained from the linear regression fit between the three measured SAI values (i.e., 80/20 at 28 days, 80/20 at 180 days and 68/20/10/2 at 28 days) and BW contents at 1 and 7 days, as well as cumulative heat values at ½, 1, 3 and 7 days. A good correlation is defined here as a linear fit yielding $R^2 > 0.75$. Consistent with previous findings [48,57,79], Table 8 shows that SAI correlates more strongly with cumulative heat than with BW. Although $\mathrm{BW}^{40\,^\circ\mathrm{C}}_{1d}$ gave better correlations that at $\mathrm{BW}^{40\,^\circ\mathrm{C}}_{7d}$ for the 80/20 blend, the R^2 values remained lower than those obtained from cumulative heat fits. As a result, correlations involving BW are not further discussed here.

Fig. 6 displays the correlations between SAI at 20 °C and cumulative heat release at 40 °C for four selected time intervals for the 80/20 blends. As previously reported for 70/30 blends [57], two distinct trends are observed: one for kaolinitic calcined clays and another for the rest of the SCMs. A novel observation from this work is that smectitic calcined clays align with the rest of the SCMs rather than with KCCs. This

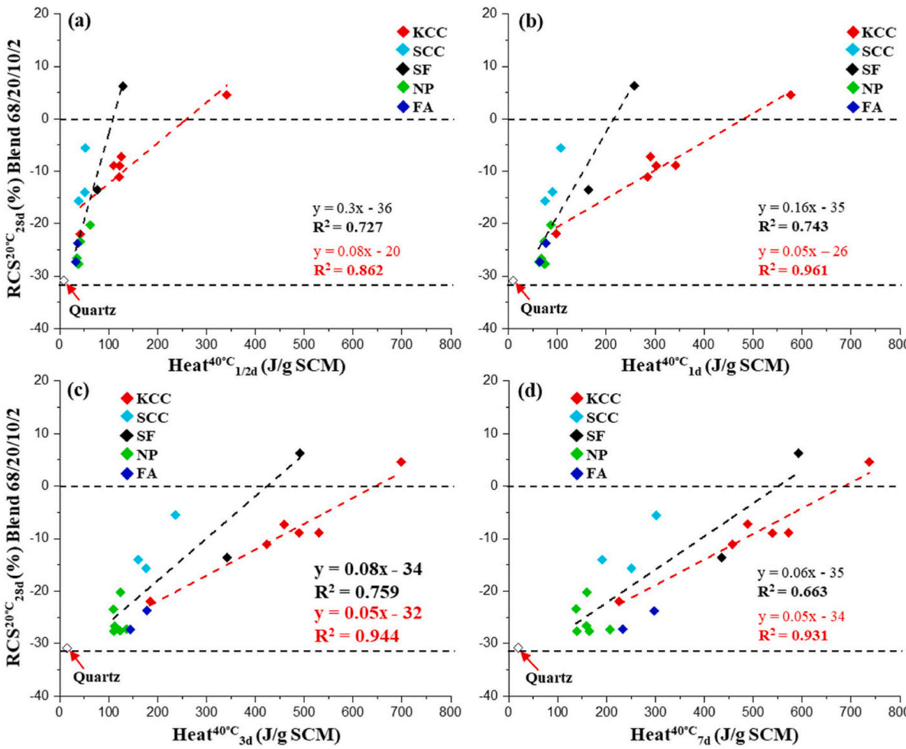

Fig. 8. Linear correlation plots of the relative compressive strength (RCS) at 20 °C for the 68/20/10/2 blends versus cumulative heat release of the corresponding SCMs, as in Fig. 6. The horizontal dashed lines indicate PC replacement levels of 0 and 32 %.

behaviour may be attributed to their moderate (reactive) Al_2O_3 content. As shown numerically in Table 8, and graphically in Fig. 6, the correlations are strongest for the heat released at ½ day for the 80/20 series, R^2 index highlighted in bold in Table 8. Heats measured at longer times yielded poorer correlations. Overall, the correlations are not very strong, with the maximum R^2 value being 0.80 for the heat release at ½ day for all SCMs except KCC, named *other SCMs*. This is likely due to the important (scattered) contribution of the filler effect. It is noteworthy that a previous study [60] reported no correlation between SAI and R^3 results. This discrepancy can likely be attributed to several factors: (1) The use of 80/20 blends, which introduce a substantial filler effect, (2) the w/b ratio was not kept strictly constant, (3) the earliest heat release measurement used for correlation was at 3 days, missing early pozzolanic activity, and (4) the $D_{V,50}$ values of the SCMs employed in that study exhibited significant variability.

Fig. 7 shows the correlation between $SAI^{20^\circ C}_{180d}$ and the $Heat^{40^\circ C}_{7d}$ for selected 80/20 blends. Interestingly, no correlation is observed between $SAI^{20^\circ C}_{180d}$ and the $Heat^{40^\circ C}_{7d}$ for KCCs, as indicated by the red diamonds in Fig. 7 and the low R^2 values in Table 8. In contrast, the correlation for *other SCMs* is acceptable, with an R^2 value of 0.77. SCCs align well within this general trend. The long-term performance of FA is particularly evident, as shown by the blue diamond in Fig. 7. At 28 days, FAs fall well below the general fit line, see Fig. 6, but surpass it significantly at 180 days in Fig. 7. Finally, it is noteworthy that both FA and SF outperform most KCCs at 180 days.

The crux of this work is graphically presented in Fig. 8, which illustrates the $SAI^{20^\circ C}_{28d}$ values plotted against $Heat^{40^\circ C}_{1/2,1,3,7d}$ for the 68/20/20/2 blends. Two distinct trends are evident, one for KCCs (red diamonds) and another for the rest of SCMs. For the KCC series, the best correlation is obtained with the heat at 1 day, $R^2 = 0.96$. For the *other SCMs* series, the best fit is obtained with the heat at 3 days, $R^2 = 0.76$. Several important observations can be made from a detailed analysis of Fig. 8: (i) Considering $Heat^{40^\circ C}_{3d}$ as optimum overall descriptor, a KCC-based SCM requires 640 J/g to achieve an SAI of 100 % at 28 days. In contrast, SCMs from the other series can achieve the same SAI of 100 % with only 430 J/g (ii) The slopes of the KCC fits change minimally with cumulative heat duration, decreasing from 0.08 to 0.05 g/J between ½ and 7 days. Conversely, the slopes for the rest of the SCMs vary significantly, declining from 0.3 to 0.06 g/J over the same period. This pronounced change may suggest a shift in the reaction mechanism for SCMs at 40 °C, but further research is needed to confirm this behaviour. (iii) As previously discussed, this blend configuration effectively identifies quartz as inert, and positions all slow-reacting commercial pozzolans above the 32 % dilution level. (iv) The, SCC results align with the second series (non-KCC SCMs). However, a closer inspection suggests that their SAI values are consistently above the general trend at 28 days. This is not surprising, as the moderate reactive aluminium content of SCCs may enhance the initial pozzolanic reaction rate. Additional independent research is required to validate this preliminary observation. (v) Most importantly, the best fits obtained here for the 68/20/10/2 blends and $Heat^{40^\circ C}_{3d}$, gave: slope = 0.05 g/J and intercept = −32 for KCC and slope = 0.08 g/J and intercept = −34 for the rest of SCMs. Interestingly, the corresponding fits for the 70/30 blends reported in Ref. [57] of RILEM showed similar findings for $Heat^{40^\circ C}_{7d}$, with a slope = 0.05 g/J and intercept = −34 for KCC, and slope = 0.10 g/J and intercept = −39 for the rest of SCMs. The similarities in the obtained values for very different SCMs seems to indicate that this is a universal correlation. If this is confirmed, it will be very helpful for predicting compressive strength ranges.

5. Conclusions

In this investigation, twenty-two SCMs, belonging to five families (i.e. kaolinite calcined clays, smectite calcined clays, silica fumes, natural pozzolans and class-F fly ashes), have been very systematically investigated with quartz included as a reference to evaluate filler effects without pozzolanicity. All final SCMs were milled to a $D_{V,50}$ target of 12 ± 2 μm to ensure comparable results. The pozzolanic performances were determined using ASTM C1897 (R^3 test) and a modified ASTM C311 test, in which the w/b ratio was kept constant at 0.50. Additionally, the strength activity index values of a second blend comprising 68 wt% PC, 20 wt% SCM, 10 wt% limestone, and 2 wt% gypsum were also measured. The following key conclusions are drawn.

5.1. Smectite calcined clays have been thoroughly investigated as they can play a key role in regions where kaolinitic clays are not locally available. These materials are more reactive than natural pozzolans but less reactive than kaolinitic-rich calcined clays. As expected based on their aluminium contents, it is shown that montmorillonites (dioctahedral — Al-rich) are more reactive than saponites (trioctahedral — Mg-rich). Moreover, Na-montmorillonites are more pozzolanic than Ca-montmorillonites. In any case, the early-age pozzolanic reaction rates are also governed by their specific surface areas, as expected. This observation represents a novel contribution of the present study.

5.2. For slow-reacting pozzolans, it is deduced that a large fraction of fine particles, here arbitrarily defined as smaller than 3 μm, enhances the pozzolanic reaction rate at early ages. As expected, larger specific surface areas also contribute to faster initial pozzolanic reaction rates.

5.3. All commercial slow-reacting pozzolans are identified as pozzolanically active using the RILEM threshold of $\mathrm{Heat}^{4^\circ C}_{7d} = 98$ J/g of SCM, 66 % confidence level. However, the 90 % confidence level threshold of 160 J/g excludes certain commercial pozzolans that achieve acceptable SAI values at later pozzolanic reaction ages.

5.4. For the 80/20 blends, the correlation between R^3 results at 7 days and the SAI value at 28 days is poor as it has been extensively discussed, primarily due to filler effects. Nonetheless, two distinct trends emerge when fitting the SAI results to the R^3 heats at 1/2 and 1 days with relatively good correlations. This is a very significant result of this study. In addition, kaolinite calcined clays group in one cluster and the rest of SCMs associate in a second trend. This differentiation has been attributed to the higher heat release from the aluminate reaction with portlandite in the presence of carbonate anions.

5.5. It is not recommended to conduct SAI investigations using 80/20 blends due to the significant scattering of results, even when the w/b ratio is fixed.

5.6. Very clear correlations are observed for 68/20/10/2 blends, when plotting $\mathrm{SAI}^{2^\circ C}_{28d}$ and $\mathrm{Heat}^{4^\circ C}$ at different times. Two distinct trends are evident, one for kaolinitic calcined clays and another for the rest of SCMs. The slopes of the linear fits for KCC vary only slightly (from 0.08 to 0.05 g/J). In contrast, the slopes for the rest of the SCMs show more significant variation (from 0.30 to 0.06 g/J). Further research is required to mechanistically understand this behaviour.

5.7. The most important conclusion is the observed general linear correlation for blends containing about 70 % of PC. The best fits obtained for the 68/20/10/2 blends, when representing $\mathrm{SAI}^{2^\circ C}_{28d}$ and $\mathrm{Heat}^{4^\circ C}_{3d}$, yielded a slope of 0.05 g/J and an intercept of −32 for KCC, while the other SCMs showed a slope of 0.08 g/J and an intercept of −34. A previous study by RILEM on 70/30 blends [57] reported similar findings for $\mathrm{Heat}^{4^\circ C}_{7d}$, showing a slope of 0.05 g/J and an intercept of −34 for KCC, whereas the other SCMs exhibited a slope of 0.10 g/J and an intercept of −39. These two studies employed very different materials. Notably, this investigation included three smectitic calcined clays and two silica fumes, which were not considered in the RILEM study. The consistency in the obtained values strongly suggests that this is a general result. Such an observation could be invaluable for predicting compressive strengths with greater accuracy.

5.1. Limitations of this study

The number of SCMs is constantly increasing and there are complete families which are not treated here such as vegetable ashes, carbonated recycled concrete fines, different types of slags, etc. The behaviours of these materials in the correlation plots are unknown to the authors. A second limitation of this work is the correlation between heat release and mechanical strength at later ages (e.g. 180 days), which remains insufficiently investigated. More efforts have to be allocated to the correlations with the compressive strengths after four months of hydration. Finally, another limitation of the present work is the lack of study of the correlation between heat release (or bound water) and durability-related properties. Compressive strengths are commonly used as a proxy for durability but this would add complexity and could decrease the relationships. A well-planned research addressing the possible correlations between SCM pozzolanic activity (as measured by ASTM C1897) and durability performances are lacking.

CRediT authorship contribution statement

Imane Koufany: Writing – review & editing, Writing – original draft, Methodology, Investigation, Formal analysis, Data curation. **Angeles G. De la Torre:** Writing – review & editing, Supervision, Investigation, Funding acquisition. **Cinthya Redondo-Soto:** Writing – review & editing, Investigation. **Isabel Santacruz:** Writing – review & editing, Supervision, Investigation, Funding acquisition. **Ana Cuesta:** Writing – review & editing, Investigation. **Daniela Gastaldi:** Writing – review & editing, Investigation. **Fulvio Canonico:** Writing – review & editing, Investigation, Conceptualization. **Oliver Mazanec:** Writing – review & editing, Investigation, Conceptualization. **Miguel A.G. Aranda:** Writing – review & editing, Writing – original draft, Supervision, Investigation, Conceptualization.

Declaration of competing interest

The authors declare that they have no competing interest.

Acknowledgements

CSA Research LLC (USA) is thanked for funding I.K. PID2020-114650RB-I00 grant from Ministry of Science and Innovation of Spain, co-funded by ERDF, is thanked for partial financial support. Escuela de Ingenierías Industriales of Universidad of Málaga is thanked for providing the devices funded by Junta de Andalucía and ERDF (IE19_182 UMA grant) to perform the mechanical strength tests. The authors thank Ms. B. Guirado-Rodríguez, Ms. E. M. Benjumea-Rejano, and Mr. F. Gómez-García for assisting with some of the SAI tests. Funding for open access charge: Universidad de Málaga/CBUA.

Annex.

Table A1
Elemental analyses of the raw clays. All data are expressed as oxide weight percentages. The loss on ignition (LOI) values are also reported.

wt%	SiO_2	Al_2O_3	Fe_2O_3	CaO	MgO	K_2O	Na_2O	Minors	S + A + F[a]	LOI*
KRC1	50.3	29.3	6.8	0.2	0.3	0.3	–	2.3	86	10.5
KRC2	60.7	24.2	2.5	0.3	0.1	0.3	–	0.2	87	10.8
KRC3	55.3	29.3	1.2	0.2	0.3	3.3	0.2	1.2	86	9.3
KRC4	54.1	30.2	1.6	0.02	0.3	4.8	0.3	0.9	86	16.0
KRC5	72.6	20.5	0.2	0.1	0.1	1.1	–	0.2	93	5.2
KRC6	76.6	14.8	0.2	0.1	0.1	1.3	–	0.2	92	6.9
KRC7	63.4	16.5	5.9	1.3	0.8	3.4	0.3	1.4	86	7.2
Ref1-SRC	58.5	18.8	4.3	>0.1	4.6	1.4	1.0	0.6	82	10.5
Ref2-SRC	62.8	19.2	3.9	1.5	2.3	0.5	1.8	0.2	86	6.8
SRC1	56.0	8.9	4.3	1.2	17.7	2.3	–	0.8	69	8.8
SRC2	55.3	14.9	5.4	9.4	3.6	1.1	1.1	0.8	76	8.3
SRC3	57.9	17.5	5.2	3.5	2.4	3.8	2.2	1.3	81	6.0

* Dried at 105 °C and heated at 950 °C for 2 h.
a S + A + F stands for the sum of SiO_2, Al_2O_3 and Fe_2O_3.

Table A2
Mineralogical compositions including ACn of the raw clays determined by RQPA and the internal standard method (using 20 wt% of Al_2O_3) all data in weight percentage.

Phases/ wt%	KRC1	KRC2	KRC3	KRC4	KRC5	KRC6	KRC7	Ref1-SRC	Ref2-SRC	SRC1	SRC2	SRC3
ACn	9	30	12	10	21	21	30	96	78	76	57	44
Kaolinite	72.9(3)	42.6(9)	57.1(5)	48.8(7)	20.3(4)	16.8(4)	8.8(1)	–	–	–	–	–
Qz	11.1(2)	27.2(4)	12.9(2)	11.4(2)	47.5(1)	53.6(1)	36.8(2)	3.9(4)	7.4(7)	3.0(5)	3.0(3)	0.6(3)
Muscovite	–	–	11.1(2)	24.9(3)	5.7(2)	3.1(2)	23.9(4)	–	–	9.7(1)	–	18.7(7)
Microcline	–	–	6.1(3)	4.2(3)	4.4(2)	4.6(2)	–	–	4.2(5)	3.7(8)	–	–
Sanidine	–	–	–	–	–	–	–	–	–	3.0(8)	–	13.2(4)
Albite	–	–	–	–	–	–	–	–	8.3(5)	–	–	4.9(7)
Andesine	–	–	–	–	–	–	–	–	–	–	–	17.6(7)
Anorthite	–	–	–	–	–	–	–	–	–	4.0(1)	25.9(5)	–
Amphibole	–	–	–	–	–	–	–	–	–	–	4.4(5)	–
Calcite	–	–	–	–	–	–	–	–	–	–	4.3(3)	–
Minors	*6.5*	*0.6*	*1.1*	*0.7*	*0.9*	*0.6*	0.5	-	*2.4*	1.1	5.5	*1.5*

#The amorphous fractions of the smectite clays contain the smectite phase content as the poor crystallinity of smectites does not allow its direct quantification by RQPA.

Table A3
Mineralogical compositions of the employed PC, quartz, limestone and gypsum.

Phases/ wt%	PC	Qz	LS	Gyp
C_3S	64.0	–	–	–
C_2S	9.5	–	–	–
C_3A	4.8	–	–	–
C_4AF	11.5	–	–	–
$C\underline{C}$	6.0	–	100	–
$C\underline{S}H_{0.5}$	1.8	–	–	–
$C\underline{S}H_2$	2.2	–	–	96.6
Qz	0.2	100	–	3.4

Table A4
Summary of regression results (R^2 coefficient and linear fits) relating the relative compressive strengths at the given curing ages with the R^3 test results (bound water and heat released) for the two studied blends series. The fits are carried out for the KCCs and o*ther SCMs (in italics)*.

			R^2	Slope	Intercept
80/20 series	RCS at 28 d	BW at 1 d	0.509/*0.512*	*3/6*	−15/*-26*
		BW at 7 d	0.338/*0.399*	*2/4*	−14/*-28*
		Heat at 1/2 d	0.611/*0.805*	0.06/*0.21*	−5/*-19*
		Heat at 1 d	0.511/*0.778*	0.04/*0.11*	−7/*-19*
		Heat at 3 d	0.433/0.646	0.03/*0.05*	−10/*-18*
		Heat at 7 d	0.412/*0.499*	0.03/*0.04*	−11/*-18*
	RCS at 180 d	BW at 1 d	0.067/*0.362*	*1/5*	−12/*-24*
		BW at 7 d	0.227/*0.540*	*2/4*	−22/*-33*
		Heat at 1/2 d	0.422/*0.505*	0.04/*0.2*	−10/*-18*
		Heat at 1 d	0.277/*0.563*	0.02/*0.10*	−12/*-18*
		Heat at 3 d	0.169/*0.677*	0.02/*0.06*	−15/*-18*
		Heat at 7 d	0.148/*0.768*	0.02/*0.05*	−15/*-20*
68/20/10/2 series	RCS at 28 d	BW at 1 d	0.900/*0.415*	*5/7*	−39/*-43*
		BW at 7 d	0.940/*0.440*	*4/6*	−42/*-50*
		Heat at 1/2 d	0.862/*0.727*	0.08/*0.3*	−20/*-36*
		Heat at 1 d	0.961/*0.743*	0.05/*0.16*	−26/*-35*
		Heat at 3 d	0.944/*0.759*	0.05/*0.08*	−32/*-34*
		Heat at 7 d	0.931/*0.663*	0.05/*0.06*	−34/*-35*

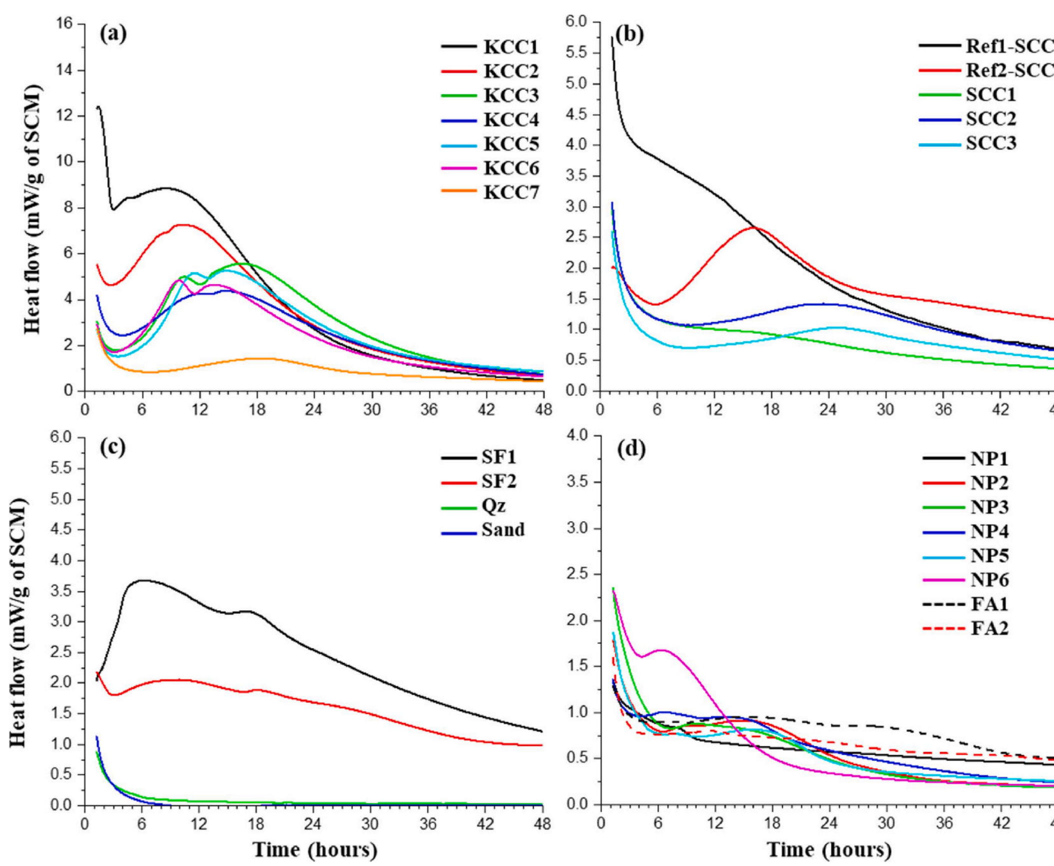

Fig. A1. Heat flow curves for the R^3 mixtures during the first 48 h of the measurements: (a) KCCs, (b) SCCs, (c) SF and inerts, and (d) NPs and FAs.

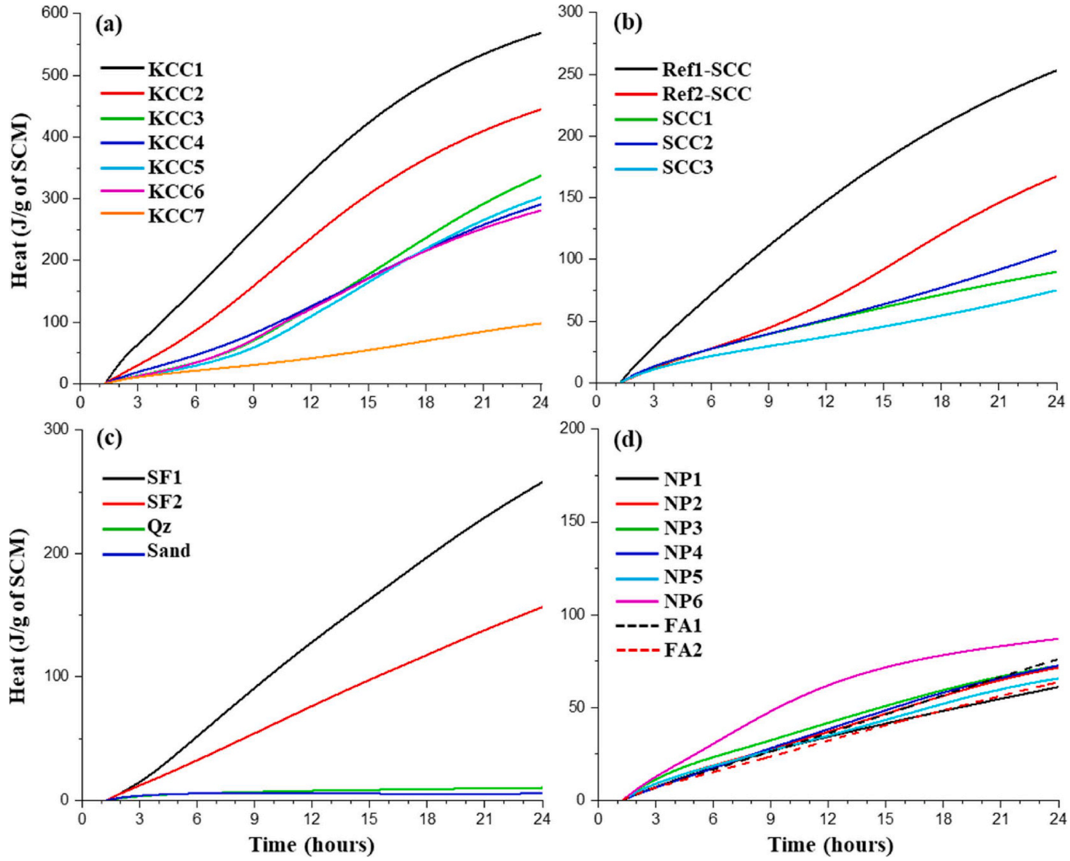

Fig. A2. Cumulative heat curves for the R^3 mixtures displayed up to 1 day for better visualisation. (a) KCCs, (b) SCCs, (c) SFs and inerts, an (d) NPs and FAs and.

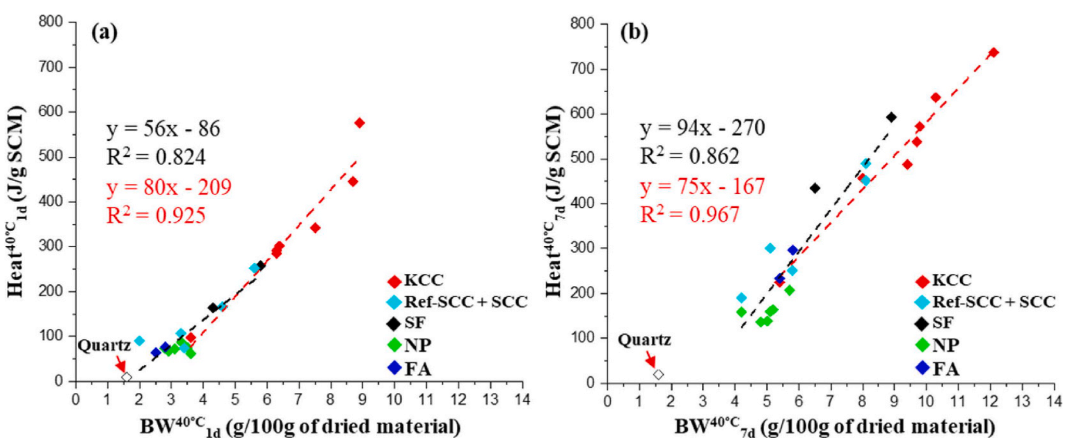

Fig. A3. Linear correlation, Heat-Bound water (R^3 test), for KCC (red diamond and red fit) and remaining SCMs (black fit). (a) Results at 1 day. (b) Results at 7 days.

Data availability

Data will be made available on request.

References

[1] S.A. Miller, R.J. Myers, Environmental impacts of alternative cement binders, Environ. Sci. Technol. 54 (2020) 677–686, https://doi.org/10.1021/acs.est.9b05550.

[2] IEA, Tracking industry 2020 – analysis. https://www.iea.org/reports/tracking-industry-2020, 2020 (accessed April 7, 2022).

[3] P. Fennell, J. Driver, C. Bataille, S.J. Davis, Cement and steel — nine steps to net zero, Nature 603 (2022) 574–577, https://doi.org/10.1038/d41586-022-00758-4.

[4] G. Habert, S.A. Miller, V.M. John, J.L. Provis, A. Favier, A. Horvath, K.L. Scrivener, Environmental impacts and decarbonization strategies in the cement and concrete industries, Nat. Rev. Earth Environ. 1 (2020) 559–573, https://doi.org/10.1038/s43017-020-0093-3.

[5] S.J. Davis, N.S. Lewis, M. Shaner, S. Aggarwal, D. Arent, I.L. Azevedo, S.M. Benson, T. Bradley, J. Brouwer, Y.M. Chiang, C.T.M. Clack, A. Cohen, S. Doig, J. Edmonds, P. Fennell, C.B. Field, B. Hannegan, B.M. Hodge, M.I. Hoffert, E. Ingersoll, P. Jaramillo, K.S. Lackner, K.J. Mach, M. Mastrandrea, J. Ogden, P.F. Peterson, D. L. Sanchez, D. Sperling, J. Stagner, J.E. Trancik, C.J. Yang, K. Caldeira, Net-zero emissions energy systems, Science 360 (2018) eaas9793, https://doi.org/10.1126/science.aas9793.

[6] S. Barbhuiya, B. Bhusan Das, D. Adak, Roadmap to a net-zero carbon cement sector: strategies, innovations and policy imperatives, J. Environ. Manag. 359 (2024) 121052, https://doi.org/10.1016/J.JENVMAN.2024.121052.

[7] R. Snellings, Assessing, understanding and unlocking supplementary cementitious materials, RILEM tech, Lett. 1 (2016) 50–55, https://doi.org/10.21809/RILEMTECHLETT.2016.12.
[8] R. Snellings, P. Suraneni, J. Skibsted, Future and emerging supplementary cementitious materials, Cement Concr. Res. 171 (2023) 107199, https://doi.org/10.1016/J.CEMCONRES.2023.107199.
[9] U.N. Environment, K.L. Scrivener, V.M. John, E. Gartner, Eco-efficient cements: potential, economically viable solutions for a low-CO2, cement-based materials industry, Cement Concr. Res. 114 (2018) 2–26, https://doi.org/10.1016/j.cemconres.2018.03.015.
[10] S.C. Pal, A. Mukherjee, S.R. Pathak, Investigation of hydraulic activity of ground granulated blast furnace slag in concrete, Cement Concr. Res. 33 (2003) 1481–1486, https://doi.org/10.1016/S0008-8846(03)00062-0.
[11] K. Scrivener, F. Martirena, S. Bishnoi, S. Maity, Calcined clay limestone cements (LC3), Cement Concr. Res. 114 (2018) 49–56, https://doi.org/10.1016/j.cemconres.2017.08.017.
[12] R. Snellings, R. Almenares Reyes, T. Hanein, E.F. Irassar, F. Kanavaris, M. Maier, A. T. Marsh, L. Valentini, F. Zunino, A. Alujas Diaz, Paper of RILEM TC 282-CCL: mineralogical characterization methods for clay resources intended for use as supplementary cementitious material, Mater. Struct. Constr. 55 (2022) 1–32, https://doi.org/10.1617/s11527-022-01973-1.
[13] A. Alujas Diaz, R.S. Almenares Reyes, T. Hanein, E.F. Irassar, M. Juenger, F. Kanavaris, M. Maier, A.T. Marsh, T. Sui, K.C. Thienel, L. Valentini, B. Wang, F. Zunino, R. Snellings, Properties and occurrence of clay resources for use as supplementary cementitious materials: a paper of RILEM TC 282-CCL, Mater. Struct. Constr. 55 (2022), https://doi.org/10.1617/s11527-022-01972-2.
[14] F. Massazza, Pozzolanic cements, Cem. Concr. Compos. 15 (1993) 185–214, https://doi.org/10.1016/0958-9465(93)90023-3.
[15] A. Játiva, E. Ruales, M. Etxeberria, Volcanic ash as a sustainable binder material: an extensive review, Materials (Basel) 14 (2021) 1–32, https://doi.org/10.3390/ma14051302.
[16] R. Snellings, G. Mertens, J. Elsen, Supplementary cementitious materials, Rev. Mineral. Geochem. 74 (2012) 211–278, https://doi.org/10.2138/rmg.2012.74.6.
[17] R. Siddique, Utilization of silica fume in concrete: review of hardened properties, Resour. Conserv. Recycl. 55 (2011) 923–932, https://doi.org/10.1016/J.RESCONREC.2011.06.012.
[18] M.I. Khan, R. Siddique, Utilization of silica fume in concrete: review of durability properties, Resour. Conserv. Recycl. 57 (2011) 30–35, https://doi.org/10.1016/J.RESCONREC.2011.09.016.
[19] K. Thienel, S. Scherb, N. Beuntner, M. Maier, R. Sposito, 1:1 or 2:1 - Does it matter for calcined clay as supplementary cementitious material?, in: Ce/Papers - Proc. Civ. Eng., 2023, pp. 363–372, https://doi.org/10.1002/cepa.2775.
[20] N. Kumari, C. Mohan, Basics of clay minerals and their characteristic properties, in: Clay Clay Miner., 2021, https://doi.org/10.5772/intechopen.97672.
[21] M. Antoni, J. Rossen, F. Martirena, K.L. Scrivener, Cement substitution by a combination of metakaolin and limestone, Cement Concr. Res. 42 (2012) 1579–1589, https://doi.org/10.1016/j.cemconres.2012.09.006.
[22] H. Maraghechi, F. Avet, H. Wong, H. Kamyab, K.L. Scrivener, Performance of Limestone Calcined Clay Cement (LC3) with various kaolinite contents with respect to chloride transport, Mater. Struct. 51 (2018) 125, https://doi.org/10.1617/s11527-018-1255-3.
[23] Y.A. Al-Noaimat, T. Akis, Influence of cement replacement by calcinated kaolinitic and montmorillonite clays on the properties of mortars, Arabian J. Sci. Eng. 48 (2023) 14043–14057, https://doi.org/10.1007/s13369-023-08041-y.
[24] T. Hanein, K.-C. Thienel, F. Zunino, A.T.M. Marsh, M. Maier, B. Wang, M. Canut, M.C.G. Juenger, M. Ben Haha, F. Avet, A. Parashar, L.A. Al-Jaberi, R.S. Almenares-Reyes, A. Alujas-Diaz, K.L. Scrivener, S.A. Bernal, J.L. Provis, T. Sui, S. Bishnoi, F. Martirena-Hernández, Clay calcination technology: state-of-the-art review by the RILEM TC 282-CCL, Mater. Struct. 55 (2021) 1–29, https://doi.org/10.1617/S11527-021-01807-6.
[25] R. Jaskulski, D. Jóźwiak-Niedźwiedzka, Y. Yakymechko, Calcined clay as supplementary cementitious material, Materials (Basel) 13 (2020) 4734, https://doi.org/10.3390/ma13214734.
[26] A. Morales-Cantero, D. Vallina, A.G. De la Torre, A. Cuesta, I. Santacruz, A. Dalla-Libera, P. Borralleras, S. Dhers, P. Schwesig, O. Mazanec, M.A.G. Aranda, Enhancing fluidity and mechanical properties in Limestone Calcined Clay cements with one-third Portland clinker content, J. Build. Eng. 95 (2024) 110334, https://doi.org/10.1016/j.jobe.2024.110334.
[27] I.M.R. Bernal, M.A.G. Aranda, I. Santacruz, A.G. De la Torre, A. Cuesta, Early-age reactivity of calcined kaolinitic clays in LC3 cements: a multi technique study including pair distribution function analysis, J. Sustain. Cem. Mater. 12 (2023) 721–735, https://doi.org/10.1080/21650373.2022.2117248.
[28] K.L. Scrivener, F. Avet, H. Maraghechi, F. Zunino, J. Ston, W. Hanpongpun, A. Favier, Impacting factors and properties of limestone calcined clay cements (LC3), Green Mater. 7 (2019) 3–14, https://doi.org/10.1680/jgrma.18.00029.
[29] F. Avet, K.L. Scrivener, Investigation of the calcined kaolinite content on the hydration of limestone calcined clay cement (LC3), Cement Concr. Res. 107 (2018) 124–135, https://doi.org/10.1016/j.cemconres.2018.02.016.
[30] L. Lei, M. Palacios, J. Plank, A.A. Jeknavorian, Interaction between polycarboxylate superplasticizers and non-calcined clays and calcined clays: a review, Cement Concr. Res. 154 (2022) 106717, https://doi.org/10.1016/j.cemconres.2022.106717.
[31] R. Fernandez, F. Martirena, K.L. Scrivener, The origin of the pozzolanic activity of calcined clay minerals: a comparison between kaolinite, illite and montmorillonite, Cement Concr. Res. 41 (2011) 113–122, https://doi.org/10.1016/j.cemconres.2010.09.013.
[32] S. Scherb, M. Maier, K. Mathias, N. Beuntner, K.C. Thienel, Reaction kinetics of calcined smectite in a clinker-free model and a synthetic cement system in comparison with selected calcined phyllosilicates, Cement Concr. Res. 189 (2025) 107766, https://doi.org/10.1016/J.CEMCONRES.2024.107766.
[33] A.T.M. Marsh, S. Krishnan, S.A. Bernal, Structural features of thermally or mechano-chemically treated montmorillonite clays as precursors for alkali-activated cements production, Cement Concr. Res. 181 (2024) 107546, https://doi.org/10.1016/j.cemconres.2024.107546.
[34] ASTM C1897-20 Standard Test Methods for Measuring the, Reactivity of supplementary cementitious materials by isothermal calorimetry and bound water measurements. https://doi.org/10.1520/C1897-20, 2020.
[35] N. Rakhimova, Montmorillonite clays in Portland clinker-reduced, non-clinker cements, and cement composites: a review, Constr. Build. Mater. 411 (2024) 134678, https://doi.org/10.1016/j.conbuildmat.2023.134678.
[36] T. Wang, S. Medepalli, Y. Zheng, W. Zhang, T. Ishida, S. Bishnoi, D. Hou, Z. Shi, Retardation effect of the pozzolanic reaction of low-calcium supplementary cementitious materials on clinker hydration at later age: effects of pore solution, foreign ions, and pH, Cement Concr. Res. 177 (2024) 107416, https://doi.org/10.1016/J.CEMCONRES.2023.107416.
[37] H.M. Hamada, F. Abed, H.Y. Binti Katman, A.M. Humada, M.S. Al Jawahery, A. Majdi, S.T. Yousif, B.S. Thomas, Effect of silica fume on the properties of sustainable cement concrete, J. Mater. Res. Technol. 24 (2023) 8887–8908, https://doi.org/10.1016/j.jmrt.2023.05.147.
[38] A.A. Ramezanianpour, Natural pozzolans, in: Cem. Replace. Mater. Prop. Durability, Sustain., Springer, Berlin, Heidelberg, 2014, pp. 1–46, https://doi.org/10.1007/978-3-642-36721-2_1.
[39] G. Cai, T. Noguchi, H. Degée, J. Zhao, R. Kitagaki, Volcano-related materials in concretes: a comprehensive review, Environ. Sci. Pollut. Res. 23 (2016) 7220–7243, https://doi.org/10.1007/s11356-016-6161-z.
[40] C. Dedeloudis, M. Zervaki, K. Sideris, M. Juenger, N. Alderete, S. Kamali-Bernard, Y. Villagrán, R. Snellings, Natural pozzolans in: RILEM state-of-the-art reports. https://doi.org/10.1007/978-3-319-70606-1_6, 2018.
[41] M.J. McCarthy, T.D. Dyer, Pozzolanas and pozzolanic materials, in: Lea's Chem. Cem. Concr., Elsevier, 2019, pp. 363–467, https://doi.org/10.1016/B978-0-08-100773-0.00009-5.
[42] F. Canonico, S. Mutke, A.P. Martín, A. Pellegrino, Opportunities and barriers of pozzolanic cements, Ce/Papers. Proc. Civ. Eng. 6 (2023) 127–139, https://doi.org/10.1002/cepa.2828.
[43] P.K. Metha, P.J. Monteiro, Concrete: Microstructure, Properties, and Materials, third ed., Mcgraw-Hill Professional, 2005.
[44] L. Medeghini, L. Calzolari, M. Botticelli, M. Di Fazio, C. De Vito, I. Pettiti, F. Bardelli, S. Mignardi, The secret of ancient Roman hydraulic mortar: the lesson learnt from the past for future cements, Cem. Concr. Compos. 148 (2024) 105484, https://doi.org/10.1016/J.CEMCONCOMP.2024.105484.
[45] M. Ahmaruzzaman, A review on the utilization of fly ash, Prog. Energy Combust. Sci. 36 (2010) 327–363, https://doi.org/10.1016/J.PECS.2009.11.003.
[46] D.K. Nayak, P.P. Abhilash, R. Singh, R. Kumar, V. Kumar, Fly ash for sustainable construction: a review of fly ash concrete and its beneficial use case studies, Clean. Mater. 6 (2022) 100143, https://doi.org/10.1016/J.CLEMA.2022.100143.
[47] T. Hemalatha, A. Ramaswamy, A review on fly ash characteristics- towards promoting high volume utilization in developing sustainable concrete, J. Clean. Prod. (2017), https://doi.org/10.1016/j.jclepro.2017.01.114.
[48] X. Li, R. Snellings, M. Antoni, N.M. Alderete, M. Ben Haha, S. Bishnoi, Ö. Cizer, M. Cyr, K. De Weerdt, Y. Dhandapani, J. Duchesne, J. Haufe, D. Hooton, M. Juenger, S. Kamali-Bernard, S. Kramar, M. Marroccoli, A.M. Joseph, A. Parashar, C. Patapy, J.L. Provis, S. Sabio, M. Santhanam, L. Steger, T. Sui, A. Telesca, A. Vollpracht, F. Vargas, B. Walkley, F. Winnefeld, G. Ye, M. Zajac, S. Zhang, K.L. Scrivener, Reactivity tests for supplementary cementitious materials: RILEM TC 267-TRM phase 1, Mater. Struct. 51 (2018) 151, https://doi.org/10.1617/s11527-018-1269-x.
[49] S. Al-Shmaisani, R.D. Kalina, R.D. Ferron, M.C.G. Juenger, Critical assessment of rapid methods to qualify supplementary cementitious materials for use in concrete, Cement Concr. Res. 153 (2022) 106709, https://doi.org/10.1016/J.CEMCONRES.2021.106709.
[50] F. Avet, X. Li, M. Ben Haha, S.A. Bernal, S. Bishnoi, Ö. Cizer, M. Cyr, S. Dolenec, P. Durdzinski, J. Haufe, D. Hooton, M.C.G. Juenger, S. Kamali-Bernard, D. Londono-Zuluaga, A.T.M. Marsh, M. Marroccoli, M. Mrak, A. Parashar, C. Patapy, M. Pedersen, J.L. Provis, S. Sabio, S. Schulze, R. Snellings, A. Telesca, M. Thomas, F. Vargas, A. Vollpracht, B. Walkley, F. Winnefeld, G. Ye, S. Zhang, K. Scrivener, Report of RILEM TC 267-TRM phase 2: optimization and testing of the robustness of the R3 reactivity tests for supplementary cementitious materials, Mater. Struct. Constr. 55 (2022) 1–14, https://doi.org/10.1617/s11527-022-01928-6.
[51] A. Parashar, A. Vollpracht, J. Haufe, R. Snellings, Y. Dhandapani, M. Santhanam, S. Dolenec, M. Marroccoli, A. Telesca, A.M. Joseph, N. Alderete, N. De Belie, P. Durdzinski, M. Ben Haha, M. Kasaniya, M. Thomas, Ö. Cizer, M. Antoni, S. Sabio, X. Li, R.D. Hooton, K.L. Scrivener, S. Bishnoi, Report of RILEM TC 267—TRM: improvement and robustness study of lime mortar strength test for assessing reactivity of SCMs, Mater. Struct. Constr. 55 (2022) 96, https://doi.org/10.1617/s11527-022-01911-1.
[52] ASTM C311, Standard test methods for sampling and testing fly ash or natural pozzolans for use in portland-cement concrete. https://doi.org/10.1520/C0311-11, 2011.
[53] ASTM C618, Standard Specification for Coal Fly Ash and Raw or Calcined Natural Pozzolan for Use in Concrete, ASTM Int. West, Conshohocken, 2022, https://doi.org/10.1520/C0618-22.2.

[54] UNE-EN 450-1, Fly Ash for Concrete-Part 1: Definition, Specifications and Conformity Criteria, 2020.
[55] Y. Wang, L. Burris, C.R. Shearer, D. Hooton, P. Suraneni, Strength activity index and bulk resistivity index modifications that differentiate inert and reactive materials, Cem. Concr. Compos. 124 (2021) 104240, https://doi.org/10.1016/J.CEMCONCOMP.2021.104240.
[56] F. Avet, R. Snellings, A. Alujas Diaz, M. Ben Haha, K.L. Scrivener, Development of a new rapid, relevant and reliable (R3) test method to evaluate the pozzolanic reactivity of calcined kaolinitic clays, Cement Concr. Res. 85 (2016) 1–11, https://doi.org/10.1016/j.cemconres.2016.02.015.
[57] D. Londono-Zuluaga, A. Gholizadeh-Vayghan, F. Winnefeld, F. Avet, M. Ben Haha, S.A. Bernal, Ö. Cizer, M. Cyr, S. Dolenec, P. Durdzinski, J. Haufe, D. Hooton, S. Kamali-Bernard, X. Li, A.T.M. Marsh, M. Marroccoli, M. Mrak, Y. Muy, C. Patapy, M. Pedersen, S. Sabio, S. Schulze, R. Snellings, A. Telesca, A. Vollpracht, G. Ye, S. Zhang, K.L. Scrivener, Report of RILEM TC 267-TRM phase 3: validation of the R3 reactivity test across a wide range of materials, Mater. Struct. Constr. 55 (2022) 1–16, https://doi.org/10.1617/s11527-022-01947-3.
[58] R. Snellings, D. Londoño-Zuluaga, K. Scrivener, Interlaboratory test program to determine the precision of the R3 test method (ASTM C1897-20) for measuring reactivity of supplementary cementitious materials, Adv. Civ. Eng. Mater. 11 (2022), https://doi.org/10.1520/ACEM20220023. ACEMF9.
[59] M. Frías, A. Alujas, A. Moreno-Reyes, J.A. Ibañez, M.V. Paredes, I. Vegas, Advances in understanding R3 chemical reactivity in various traditional and emerging pozzolans: chemical, mineralogical and calorimetric dimensions, Constr. Build. Mater. 457 (2024) 139474, https://doi.org/10.1016/J.CONBUILDMAT.2024.139474.
[60] J. Yoon, K. Jafari, R. Tokpatayeva, S. Peethamparan, J. Olek, F. Rajabipour, Characterization and quantification of the pozzolanic reactivity of natural and non-conventional pozzolans, Cem. Concr. Compos. 133 (2022) 104708, https://doi.org/10.1016/J.CEMCONCOMP.2022.104708.
[61] Y. Liu, Q. Yuan, Y. Tan, M.J. Garba, Comparative analysis and modification of evaluation methods for the pozzolanic reactivity of natural volcanic powders, J. Build. Eng. 78 (2023) 107590, https://doi.org/10.1016/J.JOBE.2023.107590.
[62] S.L. Williams, D.N. Beatty, W.V. Srubar, A small-scale thermogravimetric method to measure the chemical reactivity of supplementary cementitious materials, Cement 12 (2023) 100071, https://doi.org/10.1016/J.CEMENT.2023.100071.
[63] I. Koufany, I. Santacruz, M.-D. Rodriguez-Ruiz, E. Bescher, M.A.G. Aranda, A.G. De la Torre, Effect of alkanolamines in kaolinitic calcined clays pozzolanic reactivity, in: Proc. 16th, Int. Congr. Chem. Cem., 2023, https://doi.org/10.13140/RG.2.2.35533.20960.
[64] D. Vallina, M.D. Rodríguez-Ruiz, I. Santacruz, A. Cuesta, M.A.G. Aranda, A.G. De la Torre, Supplementary cementitious material based on calcined montmorillonite standards, Constr. Build. Mater. 426 (2024) 136193, https://doi.org/10.1016/J.CONBUILDMAT.2024.136193.
[65] A. Morales-Cantero, A.G. De la Torre, A. Cuesta, I. Santacruz, O. Mazanec, A. Dalla-Libera, S. Dhers, P. Borralleras, M.A.G. Aranda, Activation of LC3 Low-Carbon Cements by C-S-H Seeding, vol. I, Proc. 16th Int. Congr. Chem. Cem. -, 2023, pp. 247–250, https://doi.org/10.13140/RG.2.2.26594.09920.
[66] A. Cuesta, A. Morales-Cantero, A.G. De la Torre, I. Santacruz, O. Mazanec, A. Dalla-Libera, S. Dhers, P. Schwesig, P. Borralleras, M.A.G. Aranda, Activation of LC3 binders by C-S-H nucleation seeding with a new tailored admixture for low-carbon cements, Ce/Papers - Proc. Civ. Eng. 6 (2023) 446–453, https://doi.org/10.1002/cepa.2786.
[67] A.G. De la Torre, S. Bruque, M.A.G. Aranda, Rietveld quantitative amorphous content analysis, J. Appl. Crystallogr. 34 (2001) 196–202, https://doi.org/10.1107/S0021889801002485.
[68] A.C. Larson, R.B. Von Dreele, General structure analysis system (GSAS), los alamos natl, Lab. Rep. LAUR. 748 (2004) 86–748.
[69] K. Weise, L.M. Endell, N. Ukrainczyk, E. Koenders, Pozzolanic metakaolin reactivity: time-dependent influence of calcium hydroxide, alkali hydroxides, and sulfates, Constr. Build. Mater. 431 (2024) 136534, https://doi.org/10.1016/J.CONBUILDMAT.2024.136534.
[70] J. Mañosa, S. Huete-Hernández, A. Alvarez-Coscojuela, A. Maldonado-Alameda, J. M. Chimenos, Comparative study of limestone calcined clay cement produced with mechanically activated kaolin and calcined kaolin, J. Build. Eng. 97 (2024) 110748, https://doi.org/10.1016/j.jobe.2024.110748.
[71] S. Hollanders, Mineralogical Study of the Pozzolanic Properties of Calcined Clays, KU Leuven, 2017.
[72] S. Shirani, A. Cuesta, A. Morales-Cantero, I. Santacruz, A. Diaz, P. Trtik, M. Holler, A. Rack, B. Lukic, E. Brun, I.R. Salcedo, M.A.G. Aranda, 4D nanoimaging of early age cement hydration, Nat. Commun. 14 (2023) 2652, https://doi.org/10.1038/s41467-023-38380-1.
[73] I. Tole, K. Habermehl-Cwirzen, A. Cwirzen, Mechanochemical activation of natural clay minerals: an alternative to produce sustainable cementitious binders – review, Mineral. Petrol. 113 (2019) 449–462, https://doi.org/10.1007/S00710-019-00666-Y.
[74] Y. Dhandapani, T. Sakthivel, M. Santhanam, R. Gettu, R.G. Pillai, Mechanical properties and durability performance of concretes with limestone calcined clay cement (LC3), Cement Concr. Res. 107 (2018) 136–151, https://doi.org/10.1016/J.CEMCONRES.2018.02.005.
[75] K. Bharadwaj, O. Burkan Isgor, W. Jason Weiss, Pozzolanic reactivity of supplementary cementitious materials, ACI Mater. J. 120 (2023) 63–76, https://doi.org/10.14359/51738817.
[76] A.T.M. Marsh, A.P. Brown, H.M. Freeman, A. Neumann, B. Walkley, H. Pendlowski, S.A. Bernal, Mineralogical characteristics influence the structure and pozzolanic reactivity of thermally and mechano-chemically activated meta-kaolinites, J. Mater. Chem. A. 12 (2024) 24260–24277, https://doi.org/10.1039/d4ta02545h.
[77] M. Flegar, M. Serdar, D. Londono-Zuluaga, K. Scrivener, Regional waste streams as potential raw materials for immediate implementation in cement production, Materials (Basel) 13 (2020) 1–15, https://doi.org/10.3390/ma13235456.
[78] Z.T. Yao, X.S. Ji, P.K. Sarker, J.H. Tang, L.Q. Ge, M.S. Xia, Y.Q. Xi, A comprehensive review on the applications of coal fly ash, Earth-Science Rev. 141 (2015) 105–121, https://doi.org/10.1016/J.EARSCIREV.2014.11.016.
[79] S. Al-Shmaisani, R.D. Kalina, R.D. Ferron, M.C.G. Juenger, Comparison of SCM reactivity to performance in cement-based mixtures, Mater. Struct. Constr. 55 (2022) 241, https://doi.org/10.1617/s11527-022-02072-x.
[80] R.D. Kalina, S. Al-Shmaisani, R.D. Ferron, M.C.G. Juenger, False positives in ASTM C618 specifications for natural pozzolans, ACI Mater. J. 116 (2019) 165–172, https://doi.org/10.14359/51712243.
[81] D.P. Bentz, A. Durán-Herrera, D. Galvez-Moreno, Comparison of ASTM C311 strength activity index testing versus testing based on constant volumetric proportions, J. ASTM Int. 9 (2012), https://doi.org/10.1520/JAI104138.